
Gaussian Process Priors for Boundary Value Problems of Linear Partial Differential Equations

Jianlei Huang¹ Marc Härkönen² Markus Lange-Hegermann³ Bogdan Raiță¹

Abstract

Solving systems of partial differential equations (PDEs) is a fundamental task in computational science, traditionally addressed by numerical solvers. Recent advancements have introduced neural operators and physics-informed neural networks (PINNs) to tackle PDEs, achieving reduced computational costs at the expense of solution quality and accuracy. Gaussian processes (GPs) have also been applied to linear PDEs, with the advantage of always yielding precise solutions. In this work, we propose Boundary Ehrenpreis-Palamodov Gaussian Processes (B-EPGPs), a novel framework for constructing GP priors that satisfy both general systems of linear PDEs with constant coefficients and linear boundary conditions. We explicitly construct GP priors for representative PDE systems with practical boundary conditions. Formal proofs of correctness are provided and empirical results demonstrating significant accuracy improvements over state-of-the-art neural operator approaches.

1. Introduction

(Systems of) partial differential equations (PDEs) were classically solved using numerical solvers. To be able to find the solution, it needed to be unique. Hence, the PDE system needed enough initial conditions or boundary conditions to ensure this uniqueness. Some techniques for PDEs in machine learning mirror this general approach. For example, neural operators are neural networks trained to solve systems of evolution equations with initial conditions, where the neural network maps a state of the system at time t to time $t + 1$. While such approaches require only a fraction of computation time, they do not yet reach the quality of numerical solvers.

¹Georgetown University, Washington, D.C., USA. ²Liquid AI, Boston, MA, USA ³Institute Industrial IT, OWL University of Applied Sciences and Arts, Lemgo, Germany. Correspondence to: Bogdan Raiță <br607@georgetown.edu>.

Preliminary work.

A second category of research in machine learning disposes of the uniqueness and instead aims for finding a “good” solution of a PDE system that approximates some data points. An examples are physics informed neural networks (PINN) (Raissi et al., 2019), which are used as neural network models for regression with a usual regression loss and additionally a loss that the regression model satisfies the PDE system at randomly sampled locations in their domain. Also, many Gaussian processes (GPs) based models for linear PDE systems fall in this category.

GPs (Rasmussen & Williams, 2006) are the default functional prior, serve as robust regression models in the context of few data points, and provide calibrated uncertainties of predictions. The bilinear structure of the covariance of GPs is able to encode linear mathematical information in a prior, for example derivatives (Swain et al., 2016; Harrington et al., 2016). Encoding derivatives allowed to construct GPs with realizations in the solution set a given system of linear PDEs with constant coefficients (Lange-Hegermann, 2018; Jidling et al., 2017; Macêdo & Castro, 2008; Scheuerer & Schlather, 2012; Wahlström et al., 2013; Solin et al., 2018; Jidling et al., 2018; Särkkä, 2011), as long as these systems are controllable, i.e. allow for potentials. This construction is non-trivial and makes use of Gröbner bases for multivariate polynomial rings. The restriction to such controllable systems was first lifted for systems of ordinary differential equations (ODEs) (Besginow & Lange-Hegermann, 2022) and then for PDEs (Harkonen et al., 2023). All of these approaches allow machine learning for a huge and very relevant class of differential equations. Their underlying symbolic nature is not merely physics *informed*, but all regression functions and samples are *exact* solutions of the PDE system, making them physics *constrained*. Hence, such methods improve upon the accuracy of PINN methods by several orders of magnitude.

In practice, PDE systems come with both data and (initial or) boundary conditions. While controllable systems allow the inclusion of boundary conditions (Lange-Hegermann, 2021; Lange-Hegermann & Robertz, 2022) into GP approaches, at the cost of using Gröbner bases over Weyl algebra, this is not possible for the general case of linear PDE systems with constant coefficients. This paper develops an algo-

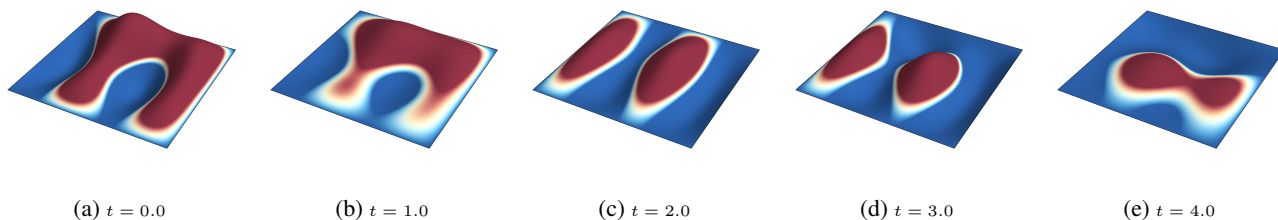


Figure 1: Consider the two-dimensional wave equation $\partial_t^2 u - \partial_x^2 u - \partial_y^2 u = 0$ with zero boundary condition on a spatial rectangle. This figure shows a sample from our Gaussian process construction B-EPGP. All samples of this Gaussian process analytically satisfy the differential equation, the boundary conditions, and can be conditioned on any finite set of data.

rhythmic construction of GP priors inside the solution set of *any* given system of (ordinary or partial) linear differential equations with constant coefficients with linear boundary conditions, which we call B-EPGP for Boundary Ehrenpreis-Palamodov Gaussian Processes. We built upon the (infinite dimensional) basis of the solution space suggested by the Ehrenpreis-Palamodov fundamental principle and map this basis to a basis of solutions of the PDE which satisfy the boundary condition.

The major contributions of this paper are as follows:

1. We give a general construction of GP priors for solutions of systems of linear PDEs with constant coefficients, including boundary conditions.
2. We explicitly construct the priors for several PDE systems with suitable boundary conditions.
3. We prove correctness and convergence properties of our construction. In particular, all our GP realizations satisfy the system of PDEs and boundary conditions.
4. We empirically demonstrate the superiority of our approach over state of the art neural operator approaches.

For the relevant code and videos, we refer to the [github](#) repository or the ancillary files of the arXiv version.

2. Gaussian Process Priors from the Ehrenpreis-Palamodov Theorem

2.1. Ehrenpreis-Palamodov Theorem

An important difference between linear and nonlinear ODE is that solutions to linear ODE systems with constant coefficients are linear combinations of exponential-polynomial solutions. If one looks at the ODE $y''' - 3y' + 2y = 0$, its exponential-polynomial solutions are of the form e^x, xe^x, e^{-2x} , where the “frequencies” 1 and -2 are the roots of the *characteristic polynomial* $z^3 - 3z + 2 = (z - 1)^2(z + 2)$.

Remarkably, this generalizes to systems of linear partial differential equations (PDE), as follows from the Ehrenpreis-Palamodov Fundamental Principle. Take the example of the 1-D heat equation, $\partial_1 u - \partial_2^2 u = 0$. Its exponential-polynomial solutions will be of the form $e^{x_1 z_1 + x_2 z_2}$, where $z_i \in \mathbb{C}$ satisfy the characteristic equation $z_1^2 - z_2^2 = 0$. This equation is obtained by replacing the partial derivative ∂_i with the polynomial variable z_i , a form of Fourier transform. We say that z lies in the *characteristic variety* $V = \{(z_1^2, z_2^2) : z_2 \in \mathbb{C}\}$. For simplicity, we state a particular case of the Ehrenpreis-Palamodov theorem.

Theorem 2.1. *Let $\Omega \subset \mathbb{R}^n$ be an open convex set. Let $A \in \mathbb{C}[\partial_1, \dots, \partial_n]$ and $V = \{z \in \mathbb{C}^n : A(z) = 0\}$. Suppose that V is an irreducible complex variety with no multiplicity. Then the linear span of $\{e^{x \cdot z}\}_{z \in V}$ is dense in the space of smooth solutions of $A(\partial)u(x) = 0$ in Ω .*

We will present this result in full generality in Appendix C, which accounts for systems, reducible varieties and multiplicities. We clarify that the solutions we construct here are $\ker_{C^\infty(\Omega)} A = \{u \in C^\infty(\Omega) : A(\partial)u = 0\}$ with its classic Fréchet topology. For the remainder of this section, we keep the assumptions of Theorem 2.1.

2.2. (Sparse) Ehrenpreis-Palamodov Gaussian Processes

(Harkonen et al., 2023) defined a Gaussian Process (GP) prior with realizations of the form $f(x) = \sum_{j=1}^r w_j e^{x \cdot z_j}$ where all “frequencies” z_j lie in the complex variety V and $w_j \sim \mathcal{N}(0, \sigma_j^2)$. This required careful local parametrization of V to enable use of SGD to optimize the z_j and σ_j^2 . We dubbed the method EPGP¹ and used it very successfully to reconstruct solutions from data at points, in some cases obtaining results of several orders of magnitude better than state of the art PINN methods.

¹(Harkonen et al., 2023) coined two terms, EPGP and S-EPGP for two different implementations of our method; here we will refer to either algorithm simply by EPGP.

3. EPGP for Boundary Value Problems

As mentioned above, EPGP excels at reconstructing solutions from given data. This has worked very well for fitting solutions to 1-D heat equation in from only 16 data points (Harkonen et al., 2023). We also obtained very accurate results in physically meaningful situations when we fitted the solutions from given initial conditions. This was the case for several examples involving the 2-D wave equation, $\partial_t^2 u - \partial_x^2 u - \partial_y^2 u = 0$.

In order to tackle realistic problems, boundary conditions must also be included in EPGP.

3.1. Naive baseline: model boundaries using data

It is also possible to incorporate boundary conditions in EPGP in the following manner. Consider for example the initial-boundary value problem for the 1-D heat equation,

$$\begin{cases} \partial_t u - \partial_x^2 u = 0 & \text{in } [0, 1] \times [-2, 2] \\ u(0, x) = f(x) & \text{for } x \in [-2, 2] \\ u(t, \pm 2) = 0 & \text{for } t \in [0, 1]. \end{cases}$$

A direct implementation of EPGP would require setting

$$u(t, x) = \sum_{j=1}^r w_j e^{z_j^2 t + z_j x}$$

for $z_j \in \mathbb{C}$ and imposing the data $u(0, X) = f(X)$ as well as $u(T, \pm 2) = 0$ for finite but large enough sets $X \subset [-2, 2]$ and $T \subset [0, 1]$. See Section F.3 for an implementation of this method for the 2-D wave equation.

This method works reasonably well in a low dimensional setting, when the boundary can be well-described by few data points due to its low volume. In higher dimension, the curse of dimensionality prevents adding enough data points to ensure suitable accuracy. Hence, this baseline falls short when compared with our new method, which imposes the boundary condition directly on the basis elements.

3.2. B-EPGP: Bases satisfying boundary conditions in halfspaces

In the first instance, we work with the simplest boundaries, i.e., halfspaces. In fact, by a change of variable, we can choose $\Omega = \mathbb{R}_+^n := \mathbb{R}^{n-1} \times [0, \infty)$. We will later generalize this approach to more general boundaries and show examples in these general cases.

We construct GP priors with realizations which satisfy

$$\begin{cases} A(\partial)u = 0 & \text{in } \mathbb{R}^{n-1} \times [0, \infty) \\ B(\partial)u = 0 & \text{on } \mathbb{R}^{n-1} \times \{0\}, \end{cases} \quad (1)$$

where $B \in \mathbb{C}[\partial]^{h \times 1}$ is a linear PDE operator which represents the boundary conditions. Starting with EPGP (cf.

Theorem 2.1) any realization

$$f(x) = \sum_{j=1}^r w_j e^{x \cdot z_j}$$

in the set of solutions of (1) should also satisfy the boundary condition *exactly*. In contrast, the naive baseline from Section 3.1 satisfies the boundary condition *approximately*.

Write $x = (x', x_n)$ where $x' \in \mathbb{R}^{n-1}$, $x_n \in \mathbb{R}$. Setting $x_n = 0$ in $B(z)f = 0$ leads to the algebraic condition

$$\sum_{j=1}^r w_j B(z_j) e^{x' \cdot z_j'} = 0 \text{ for all } x' \in \mathbb{R}^{n-1},$$

where z_j' denotes the first $n-1$ components of z_j . For this to hold, we must have that z_j' is constant with respect to j . Hence, $\sum_{j=1}^r w_j B(z_j) = 0$ for all $x' \in \mathbb{R}^{n-1}$. This enables us to write an algorithm to construct basis elements for solutions of (1).

Let $z' \in \mathbb{C}^{n-1}$ be such that there exists $z_n \in \mathbb{C}$ for which $(z', z_n) \in V$. Let V' be the set of such z' , i.e., the projection of the characteristic variety V on \mathbb{C}^{n-1} . Denote by $S_{z'} = \{z \in V : z = (z', z_n) \text{ for some } z_n \in \mathbb{C}\}$ the non-empty fibers of this projection, which can be computed by non-trivial Gröbner basis methods (Barakat & Lange-Hegermann, 2022). Then find $w_z \in \mathbb{C}$ such that

$$\sum_{z \in S_{z'}} w_z B(z) = 0. \quad (2)$$

The set of possible w_z are the left syzygies when vertically stacking the matrices $B(z)$ for $z \in S_{z'}$. These syzygies are computable by standard Gröbner basis algorithms.

We obtain the basis

$$\left\{ \sum_{z \in S_{z'}} w_z B(z) e^{x \cdot z} : \sum_{z \in S_{z'}} w_z B(z) = 0 \right\}_{z' \in V'}. \quad (3)$$

The basis (3) can be computed *explicitly* by hand for the heat and wave equations with either Dirichlet or Neumann boundary conditions.

Example 3.1 (Dirichlet boundary condition). If we set $B = 1$, we will obtain $\sum w_z = 0$ in (2). This is a broadly used condition with which we can solve explicitly. \triangle

Example 3.2. Consider the 1-D heat equation $\partial_t u - \partial_x^2 u = 0$ with Dirichlet boundary condition, $B = 1$ and $u(t, 0) = 0$. Start with $z = (\zeta^2, \zeta) \in V$ and note that $z' = \zeta^2$, so that $S_{z'} = \{\pm \zeta\}$. We conclude that in this case the basis elements are $\{e^{t\zeta^2 + x\zeta} - e^{t\zeta^2 - x\zeta}\}_{\zeta \in \mathbb{C}}$. \triangle

Example 3.3. Similarly, for the 2-D wave equation $\partial_t^2 u - \partial_x^2 u - \partial_y^2 u = 0$ with Dirichlet boundary condition $u(t, 0, y) = 0$, we obtain the basis elements $\{e^{\pm \sqrt{a^2 + b^2} t + ax + by} - e^{\pm \sqrt{a^2 + b^2} t - ax + by}\}_{a, b \in \mathbb{C}}$. \triangle

Example 3.4 (Neumann boundary condition). Another widely used boundary condition is Neumann, i.e., $B(z) = z_n$, which leads to $\sum w_z z_n = 0$. Comparing to the previous examples, this leads to the basis $\{e^{t\zeta^2+x\zeta} + e^{t\zeta^2-x\zeta}\}_{\zeta \in \mathbb{C}}$ for 1-D heat equation (Example 3.2) and $\{e^{\sqrt{a^2+b^2}t+ax \pm by} + e^{\sqrt{a^2+b^2}t+ax \mp by}\}_{a,b \in \mathbb{C}}$ for 2-D wave equation (Example 3.3). \triangle

These calculations can be performed in arbitrary dimensions and for arbitrary hyperplanes, see Appendix A. This basis replaces the basis of exponential functions in EPGP. Importantly, we can prove that our method constructs approximations of all solutions to the boundary value problem:

Theorem 3.5. *The linear span of (3) is dense in the space of all solutions of (1) for the heat or wave equation and Dirichlet or Neumann boundary conditions.*

We will prove this in Appendix B, see Appendix C for details on the topology with respect to which we have density. Relevant computational results are in Sections 4 and 5.1.

This method has substantial advantages over the direct method in Section 3.1. First, we construct solutions which satisfy the boundary condition exactly, not approximately; this improves precision and reduces the risk of overfitting. Second, no additional data points are necessary to model the boundary conditions; this improves computation time. Our numerical experiments demonstrate this clearly.

3.3. B-EPGP with linear boundaries

We extend B-EPGP to more general polygonal boundaries. Consider the following computational steps to generate a basis for the solutions set given boundary conditions with multiple halfspaces with boundaries H_k .

Step 1. Perform an affine change of variable to obtain relations (3) for each H_k . This will also give k varieties V'_k . At this point, we can turn every $e^{z \cdot x}$ with $z \in V$ into a vector space $\{\sum_j c_{k,j} e^{z_{k,j} \cdot x} : c_{k,j} \text{ satisfy (2) for } H_k\}$. Write $b_k(z)$ for a basis of this space and let $b(z) = \bigcup_k b_k(z)$. Write $\varphi(z)$ for all frequencies which appear in $b(z)$.

Step 2. IF all elements of $b(z)$ satisfy the boundary condition, THEN stop. ELSE repeat Step 2 for each $\zeta \in \varphi(z)$.

These computational steps do not terminate in general. However, if the reflection group generated by the H_k is finite, this process obviously terminates. An important case where this reflection group is finite is the case of all boundaries being orthogonal to each other. We consider cases of infinite reflection groups below in Example 3.7, where we can still construct a basis. In all remaining examples below, these computational steps terminate.

Example 3.6 (Wedge). We consider the 2-D wave equation with Dirichlet boundary condition at $x = 0$ and Neumann

boundary condition at $y = 0$:

$$\begin{cases} \square u(x, y, t) = 0 & (x, y) \in (0, \infty)^2, t > 0 \\ u(0, y, t) = 0 & y \in (0, \infty), t > 0 \\ u_y(x, 0, t) = 0 & x \in (0, \infty), t > 0 \end{cases}$$

The EPGP basis in full space for $\square u = 0$ is given by

$$\{e^{\alpha x + \beta y + \tau t} : \alpha, \beta, \tau \in \mathbb{C}, \alpha^2 + \beta^2 = \tau^2\}.$$

Performing the algorithm from the beginning of the section leads to the basis:

$$e^{\alpha x + \beta y + \tau t} - e^{-\alpha x + \beta y + \tau t} + e^{\alpha x - \beta y + \tau t} - e^{-\alpha x - \beta y + \tau t},$$

which satisfies both boundary conditions at once. Both the calculation of the basis and an implementation are described in Appendix G.2. \triangle

Example 3.7 (Infinite slab). Consider the 1-D wave equation on a line segment $(0, \pi)$ with Dirichlet boundary at both $x = 0$ and $x = \pi$,

$$\begin{cases} u_{tt} = u_{xx} & x \in (0, \pi), t \in \mathbb{R} \\ u(0, t) = u(\pi, t) = 0 & t \in \mathbb{R}. \end{cases} \quad (4)$$

An EPGP basis for the equation in full space is $e^{\sqrt{-1}\xi(x \pm t)}$ for $\xi \in \mathbb{R}$. To construct a basis that also adheres to the boundary condition at $x = 0$, we use Section 3.2 to obtain $e^{\pm \sqrt{-1}\xi t} \sin(\xi x)$. Choosing $\xi \in \mathbb{Z}$ gives a basis which satisfies the condition at $x = \pi$ as well. Both the calculation of the basis and an implementation are described in Appendix G.1. \triangle

Concerning Example 3.7, we have:

Theorem 3.8. *B-EPGP gives $\{e^{\sqrt{-1}jx} \sin(jx)\}_{j \in \mathbb{Z}}$ as a basis for (4). Its span is dense in the solution space of (4).*

Example 3.9 (Rectangle). Consider the equation in Example 3.6 in a square with Dirichlet boundary conditions:

$$\begin{cases} \square u = 0 & \text{for } x, y \in (0, \pi), t > 0 \\ u = 0 & \text{if } x \text{ or } y = 0 \text{ or } \pi. \end{cases} \quad (5)$$

In a similar fashion to Example 3.7, B-EPGP can be used to arrive at the basis

$$e^{\pm \sqrt{-1}\sqrt{j^2+k^2}t} \sin(kx) \sin(jy) \quad \text{for } j, k \in \mathbb{Z}. \quad (6)$$

In this case we retrieve the method of separation of variables (Fourier series approach). The calculation of the basis and an implementation are described in Appendix F.1. \triangle

Theorem 3.10. *B-EPGP gives the basis (6) for (5). The span of (6) is dense in the solution space of (5).*

In Theorem B.1 we will give a general statement which incorporates both Theorems 3.8 and 3.10.

3.4. Hybrid B-EPGP

In its current form, B-EPGP can be implemented with varying degrees of effort for many linear boundary conditions. For purely curved surfaces, we can use the direct method in Section 3.1 to obtain less accurate results. For domains which have both curved and flat pieces of the boundary, we can use B-EPGP to fulfill the linear boundary conditions and sample data at the curved pieces.

Example 3.11 (Sector). Consider the space-time domain $\Omega = \{(x, y, t) : x^2 + y^2 < 1, x > 0, y > 0, t > 0\}$ which has the spatial boundary $\Gamma = ([0, 1] \times \{0\}) \cup (\{0\} \times [0, 1]) \cup \{(\cos \theta, \sin \theta) : \theta \in [0, \pi/2]\}$, represented in Figure 2.

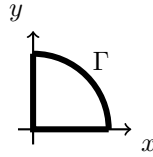


Figure 2: Circular sector in the two space directions of Ω delimited by the boundary Γ , as used in Example 3.11.

We consider the 2-D wave equation in this circular sector

$$\begin{cases} \square u = 0 & \text{in } \Omega \\ u = 0 & \text{on } \Gamma. \end{cases}$$

To account for the flat pieces of Γ , B-EPGP gives a basis similar to the one in Example 3.6, namely

$$e^{\alpha x + \beta y + \tau t} - e^{-\alpha x + \beta y + \tau t} - e^{\alpha x - \beta y + \tau t} + e^{-\alpha x - \beta y + \tau t},$$

where $\alpha, \beta, \tau \in \mathbb{C}$ and $\alpha^2 + \beta^2 = \tau^2$. To account for the circular piece, we sample many points $(\cos \theta, \sin \theta, t)$ and restrict our Gaussian process to satisfy $u = 0$ at those points. An implementation can be found in Appendix 5.3. \triangle

4. Experimental Comparison to the State of the Art

We want to compare with the Neural Operators from (Raonic et al., 2024), namely CNO and FNO. The specific experiment setting we use is 1-D wave equation with Neumann boundary condition:

$$\begin{cases} u_{tt} = u_{xx} & \text{in } (0, \infty) \times (0, \infty) \\ u(0, x) = h_1(x) & \text{for } x \in [0, \infty) \\ \frac{\partial}{\partial t} u(0, x) = h_2(x) & \text{for } x \in [0, \infty) \\ \frac{\partial}{\partial x} u(t, 0) = 0 & \text{for } t \in (0, \infty) \end{cases}$$

where $h_1(x) = f(x-3) + f(x+3) + g(x-1) + g(x+1)$ and $h_2(x) = f'(x-3) - f'(x+3)$ for $f(x) = e^{-5x^2}$,

Table 1: This table shows the median pointwise absolute and relative L_2 error in $[0, 4] \times [0, 8]$ for the experimental setting described in Section 4.

Algorithm	Absolute L1 Error		Relative L1 Error	
	n=121	n=1201	n=121	n=1201
CNO	7.24e-3	1.05e-3	1.31%	0.79%
FNO	1.05e-2	3.13e-3	1.95%	1.17%
EPGP	2.36e-4	6.62e-5	0.52%	0.14%
B-EPGP (ours)	1.96e-4	3.41e-5	0.37%	0.06%

$g(x) = e^{-10x^2}$. The exact solution is given by

$$\begin{aligned} u(x, t) &= f(x+t-3) + f(x-t+3) \\ &+ \frac{1}{2}g(x+t-1) + \frac{1}{2}g(x-t-1) \\ &+ \frac{1}{2}g(x+t+1) + \frac{1}{2}g(x-t+1) \\ &= e^{-5(x+t-3)^2} + e^{-5(x-t+3)^2} \\ &+ \frac{1}{2}e^{-10(x+t-1)^2} + \frac{1}{2}e^{-10(x-t-1)^2} \\ &+ \frac{1}{2}e^{-10(x+t+1)^2} + \frac{1}{2}e^{-10(x-t+1)^2}. \end{aligned}$$

For B-EPGP, we can easily implement the Neumann boundary into our basis, which means our basis is:

$$\{e^{\alpha(x \pm t)} + e^{\alpha(-x \pm t)}\}_{\alpha \in \mathbb{C}}.$$

See Appendix A for details on how to calculate the basis. We consider both having $n = 121$ and $n = 1201$ sample points from initial condition on the interval $[0, 12]$, and for EPGP, CNO and FNO, we sample a point on the boundary at the interval of 0.2. We show that B-EPGP is between one and two orders of magnitude superior to the neural operator methods in Table 1.

5. Examples

In this section we report the results of some of our most relevant examples outlined theoretically in Section 3. Results for the other examples in Section 3 and more can be found in Appendices F.1, F.2, F.3, G.1, G.3, H, I.

There are two main ways in which we check the accuracy of our numerical solutions:

- Verify our solvers in contexts when we know the unique true solutions to the PDEs.
- Check the conservation of energy for the wave equation in bounded domains (see Appendix E).

The latter is an important physical property which guarantees that both the equation and the (Dirichlet or Neumann) boundary conditions are satisfied.

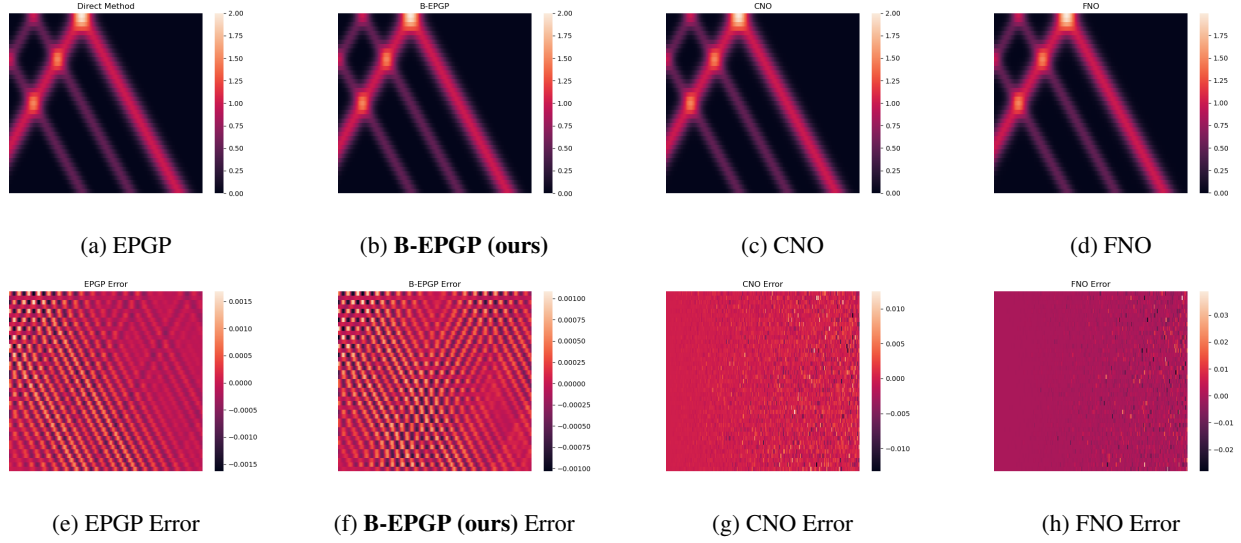


Figure 3: Estimated solution of 1-D wave equation with Neumann boundary condition on the top part of the domain. This condition represents the reflection of the wave by the boundary. We use $n = 1201$ and four different algorithms out of which ours perform better by at least one order of magnitude. We stress that the error in the neural operator approaches increases over time, whereas the error in B-EPGP stays almost constant.

In Section 4 we saw that our old algorithm EPGP and our new algorithm B-EPGP perform much better than the state of the art. In the following examples, we will compare EPGP and B-EPGP directly.

5.1. Comparison between B-EPGP and EPGP

Consider the following initial boundary value problem for the 2-D wave equation in a halfspace $x > 0$:

$$\begin{cases} u_{tt} = u_{xx} + u_{yy} & \text{for } t \in (0, \infty), x \in (0, \infty), y \in \mathbb{R} \\ u(0, x, y) = f(x, y) & \text{for } x \in [0, \infty), y \in \mathbb{R} \\ \frac{\partial}{\partial t} u(0, x, y) = 0 & \text{for } x \in [0, \infty), y \in \mathbb{R} \\ \frac{\partial}{\partial x} u(t, 0, y) = 0 & \text{for } t \in (0, \infty), y \in \mathbb{R} \end{cases}$$

with initial condition $f = f_1 + f_2 + f_3$ for

$$\begin{aligned} f_1(x, y) &= J_0(5\sqrt{((x-1)^2 + (y-1)^2)}) \\ &\quad + J_0(5\sqrt{((x+1)^2 + (y-1)^2)}), \\ f_2(x, y) &= J_0(10\sqrt{((x-2)^2 + (y-2)^2)}) \\ &\quad + J_0(10\sqrt{((x+2)^2 + (y-2)^2)}), \\ f_3(x, y) &= J_0(5\sqrt{((x-3)^2 + (y-3)^2)}) \\ &\quad + J_0(5\sqrt{((x+3)^2 + (y-3)^2)}), \end{aligned}$$

where J_0 is the Bessel function of order 0.

For this problem, the unique exact solution is given by

$$u(t, x, y) = f_1(x, y) \cos(5t) + f_2(x, y) \cos(10t)$$

Table 2: The following results from Section 5.1 show the superiority of our approach B-EPGP over EPGP when comparing both the median L1-difference to the *exact* solution and the computation time. We perform ten repetitions and report the standard deviation.

Algorithm	Abs Err(10^{-4})	Rel Err(%)	Time(s)
EPGP	4.26 ± 0.21	1.82 ± 0.09	6059
B-EPGP (ours)	0.48 ± 0.02	0.72 ± 0.03	804

$$+ f_3(x, y) \cos(5t)$$

We can use B-EPGP to obtain a basis which satisfies both the Neumann boundary condition at $x = 0$ but also the initial speed at $t = 0$, cf. Example 3.6:

$$e^{\alpha x + \beta y + \tau t} + e^{-\alpha x + \beta y + \tau t} + e^{\alpha x + \beta y - \tau t} + e^{-\alpha x + \beta y - \tau t},$$

where $\alpha, \beta, \tau \in \mathbb{C}$ and $\alpha^2 + \beta^2 = \tau^2$.

We fix the number of basis elements to be the same. Hence, the number of parameters needed to be trained in the B-EPGP approach is reduced by a factor of 4 times over those of EPGP. Furthermore, the data on the boundary in EPGP increases the covariance matrix by a factor of 9, since both initial data, initial speed and boundary data need is necessary. This triggers a significant improvement on both the running time and memory requirement. The results of B-EPGP in comparison to EPGP are shown in Table 2. A one-sided Paired Wilcoxon Signed Rank Test, with alternative hypothesis: true location shift is less than 0, shows that

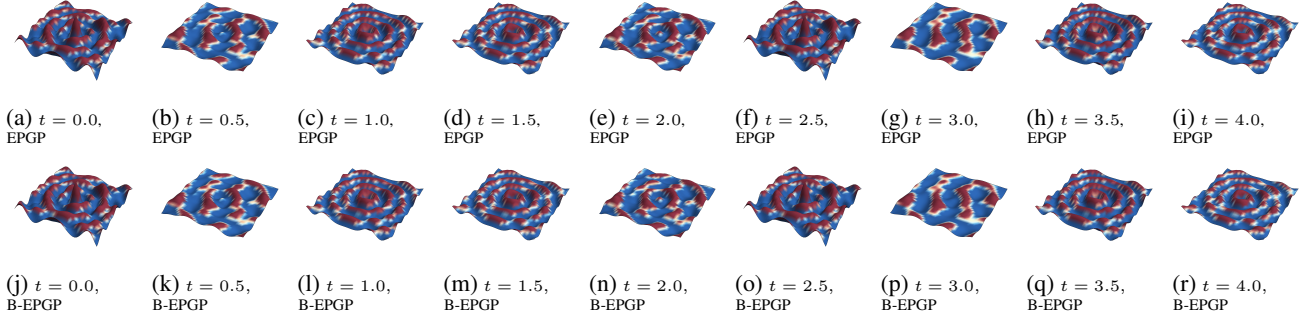


Figure 4: Predictions to the 2-D wave equation with Neumann boundary on a halfspace made using EPGP and B-EPGP. We use this experiment as a benchmark as we can compare both predictions with a highly nontrivial *exact* solution. Table 2 shows that B-EPGP is better by an order of magnitude in both accuracy and computational time. Animations can be found in the ancillary files `2DBessel-S.mp4` and `2DBessel-R.mp4`.

B-EPGP has a highly significant improvement with p -value of $0.0009766 \ll 0.05$. In this experiment, B-EPGP reduces both running times and memory cost by one order of magnitude, while also improving the quality of the results by one order of magnitude.

5.2. Wave in 3D

The 3-D wave equation is computationally challenging even without boundary conditions (see Appendix D which is concerned with adjusting EPGP to fit both initial condition and speed and comparison with the literature).

We use B-EPGP for 3-D wave equation with Neumann boundary condition on the planes $y = 0$ and $z = 0$ and initial conditions as follows.

$$\begin{cases} u_{tt} = u_{xx} + u_{yy} + u_{zz} & \text{for } x \in \mathbb{R}, y, z, t > 0 \\ u = e^{-5r_1^2} + e^{-5r_2^2} + e^{-5r_3^2} & \text{at } t = 0 \\ u_t = 0 & \text{at } t = 0 \\ u_y = 0 & \text{at } y = 0 \\ u_z = 0 & \text{at } z = 0 \end{cases}$$

where r_1, r_2, r_3 denote Euclidean distances between (x, y, z) and $(1, 1, 1), (1, -1, 1), (1, 1, -1)$, respectively.

The B-EPGP basis we use is

$$\begin{aligned} & e^{ax+by+cz+dt} + e^{ax-by+cz+dt} + e^{ax+by-cz+dt} \\ & + e^{ax-by-cz+dt} + e^{ax+by+cz-dt} + e^{ax-by+cz-dt} \\ & + e^{ax+by-cz-dt} + e^{ax-by-cz-dt} \end{aligned}$$

which can be computed using the ideas in Section G.2.

There are not many other papers which tackle this and we suspect that computation of solutions for PDE in 4-dimensions incurs a curse of dimensionality. For instance, EPGP goes out of memory on an Nvidia A100 80GB. Other related papers either do not tackle wave equations with

boundary conditions (Henderson et al., 2023) or do not tackle PDEs in 4-D (Raonic et al., 2024). In turn, our B-EPGP finishes with a low L1-error of 0.00088.

5.3. Hybrid B-EPGP in a circular sector

We will also implement our Hybrid B-EPGP method from Section 3.4 for the 2-D wave equation in a circular sector, see Example 3.11. Let $\Omega = \{x, y > 0, x^2 + y^2 \leq 4\}$ and $t \in (0, 4)$. The equations are:

$$\begin{cases} u_{tt} - (u_{xx} + u_{yy}) = 0 & \text{in } (0, 4) \times \Omega \\ u(0, x, y) = f(x, y) & \text{in } \Omega \\ u_t(0, x, y) = 0 & \text{in } \Omega \\ u_x(t, 0, y) = 0 & \text{on } (0, 4) \times \{0\} \times (0, 2) \\ u_y(t, x, 0) = 0 & \text{on } (0, 4) \times (0, 2) \times \{0\} \\ u(t, x, y) = 0 & \text{on } x^2 + y^2 = 4, \end{cases}$$

where $f(x, y) = 5 \exp(-10((x-1)^2 + (y-1)^2))$. In short, we set Dirichlet boundary conditions on the arc and Neumann boundary conditions on the wedge $xy = 0$.

These boundary conditions on the flat and curved pieces of the boundary are dealt with separately in our algorithm. To account for the Neumann boundary condition on $\{x = 0\}$ and $\{y = 0\}$ we use the B-EPGP basis for a wedge

$$e^{at+bx+cy} + e^{at-bx+cy} + e^{at+bx-cy} + e^{at-bx-cy}$$

which can be calculated using the ideas of Section G.2. To account for the Dirichlet boundary condition on the circular arc $\Gamma = \{x^2 + y^2 = 4, x, y > 0\}$, we simply assign data $u(t_h, x_h, y_h) = 0$ at many data points $(t_h, x_h, y_h) \in \Gamma$.

Snapshots of our solution are presented in Figure 7 and the conservation of energy is demonstrated in Figure 6. We iterate that the conservation of energy over time is equivalent to our prediction satisfying *both* the equation and the boundary condition exactly, see Appendix E.

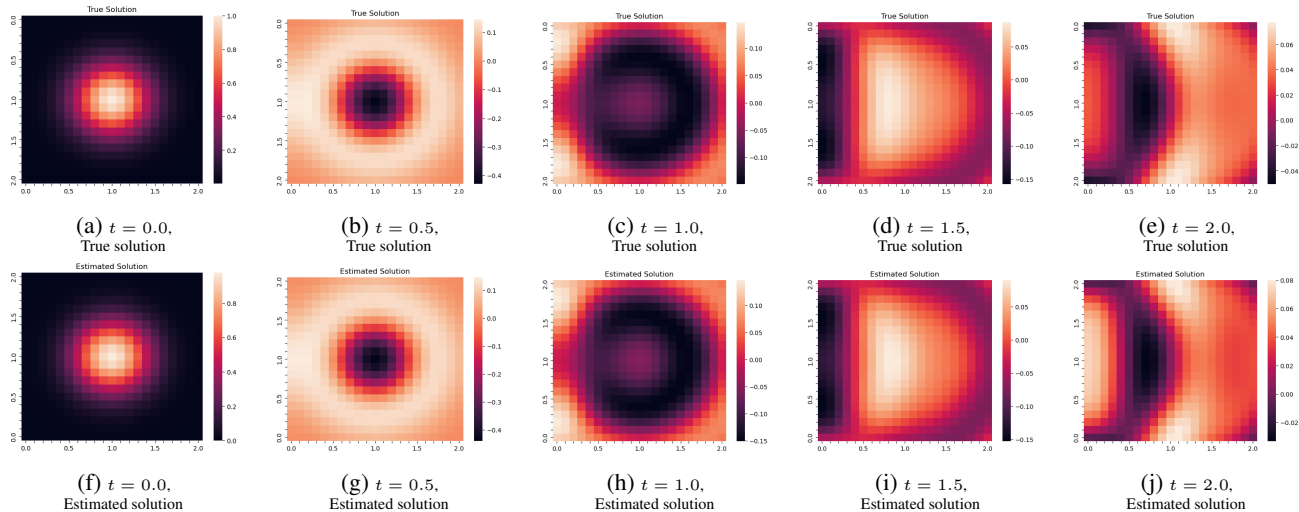


Figure 5: Visual comparison between the true solution and B-EPGP prediction for the 3-D wave equation with Neumann boundary conditions on a halfspace. We did not find competing results using Machine Learning techniques for this classic problem. Our older EPGP algorithm ran out of memory on an Nvidia A100. The snapshots are taken in the plane $y = 1$.

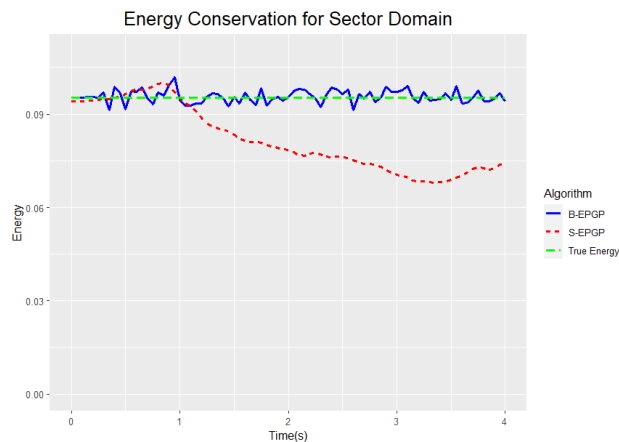


Figure 6: Proof of energy conservation for the 2-D wave equation in a sector domain. It is clear that our old method S-EPGP leads to dissipation of energy. The Hybrid B-EPGP method performs much better; its error is partly due to our approximation of the energy integral in Appendix E.

5.4. Sampling solutions from data

Our B-EPGP method yields a valid Gaussian process and is hence fully probabilistic. In addition to dealing with noisy data, it can be used to sample solutions of linear PDEs that do not uniquely determined a solution, despite having boundary conditions. This sampling can also be done in the context of given data (noisy or not) of the solution of the

PDE. For example, we consider

$$\begin{cases} u_{tt} - u_{xx} - u_{yy} = 0 & \text{for } x, y > 0 \\ u = 0 & \text{on } x = 0 \text{ and } y = 0 \end{cases}$$

and assume given arbitrary data points $(T, X, Y, U) \in \mathbb{R}^{D \times 4}$ where $D = 25$. These are arbitrary $(T, X, Y) \in [0, 4]^3$ and $U \in [-10, 10]$. We plot snapshots of two random solutions generated using B-EPGP at 5 timepoints in Figure 8, cf. Appendix G.2. This shows the flexibility of our methods when only limited data is available; for comparison, the examples we showed so far are sampled from “enough” data in contexts where the PDE is further constrained to admit unique solution.

References

Barakat, M. and Lange-Hegermann, M. An algorithmic approach to Chevalley’s theorem on images of rational morphisms between affine varieties. *Mathematics of Computation*, 91(333):451–490, 2022.

Besginow, A. and Lange-Hegermann, M. Constraining Gaussian Processes to Systems of Linear Ordinary Differential Equations. In *NeurIPS*. 2022.

Harkonen, M., Lange-Hegermann, M., and Raita, B. Gaussian process priors for systems of linear partial differential equations with constant coefficients. In *ICML*, 2023.

Harrington, H. A., Ho, K. L., and Meshkat, N. Differential algebra for model comparison. 2016. [arXiv:1603.09730](https://arxiv.org/abs/1603.09730).

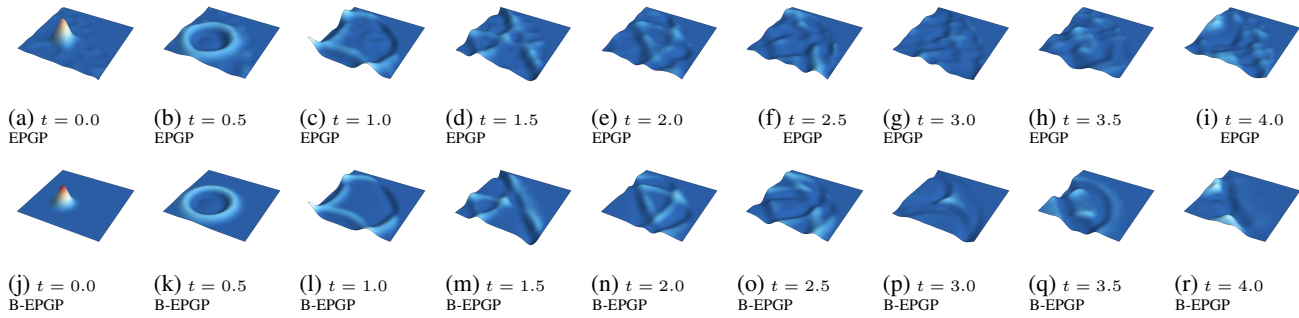


Figure 7: Solution of 2-D wave equation in a sector domain calculated using the Hybrid B-EPGP method. The superiority of B-EPGP over EPGP is visually striking and is further evidenced by the energy plot in Figure 6. Animations can be found in the ancillary files `sector.mp4` and `sectorEPGP.mp4`.

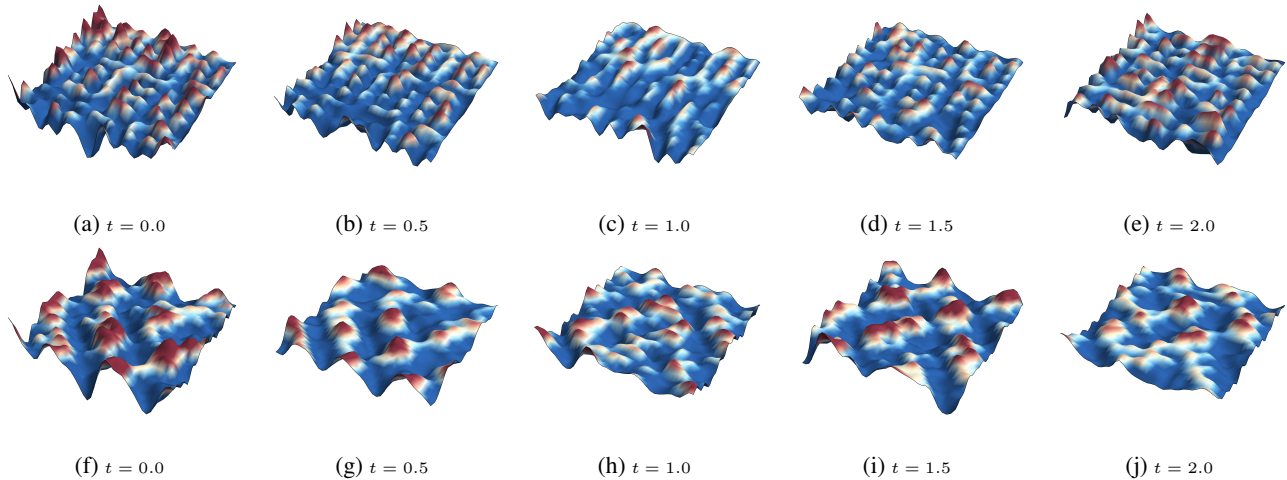


Figure 8: Irregular/noisy solutions of the 2-D wave equation with Neumann boundary conditions in a quadrant which result from sampling at only 25 data points. The data points are chosen arbitrarily and are the same for both plots. Animations can be found in the ancillary files `random1.mp4` and `random2.mp4`.

Henderson, I., Noble, P., and Roustant, O. Wave equation-tailored Gaussian process regression with applications to related inverse problems. *hal-03941939*, 2023.

Jidling, C., Wahlström, N., Wills, A., and Schön, T. B. Linearly Constrained Gaussian Processes. In *NeurIPS*, 2017.

Jidling, C., Hendriks, J., Wahlström, N., Gregg, A., Schön, T. B., Wensrich, C., and Wills, A. Probabilistic Modelling and Reconstruction of Strain. *Nuclear Instruments and Methods in Physics Research Section B: Beam Interactions with Materials and Atoms*, 2018.

Lange-Hegermann, M. Algorithmic Linearly Constrained Gaussian Processes. In *NeurIPS*. 2018.

Lange-Hegermann, M. Linearly constrained Gaussian processes with boundary conditions. In *AISTATS*, 2021.

Lange-Hegermann, M. and Robertz, D. On boundary conditions parametrized by analytic functions. In *Computer Algebra in Scientific Computing*, 2022.

Macêdo, I. and Castro, R. Learning Divergence-free and Curl-free Vector Fields with Matrix-valued Kernels. *Instituto Nacional de Matemática Pura e Aplicada, Brasil, Tech. Rep*, 2008.

Raissi, M., Perdikaris, P., and Karniadakis, G. E. Physics-informed neural networks: A deep learning framework for solving forward and inverse problems involving nonlinear partial differential equations. *Journal of Computational physics*, 2019.

Raonic, B., Molinaro, R., De Ryck, T., Rohner, T., Bartolucci, F., Alaifari, R., Mishra, S., and de Bézenac, E. Convolutional neural operators for robust and accurate learning of pdes. *Advances in Neural Information Processing Systems*, 36, 2024.

- Rasmussen, C. E. and Williams, C. K. I. *Gaussian processes for machine learning*. MIT Press, Cambridge, MA, 2006.
- Särkkä, S. Linear Operators and Stochastic Partial Differential Equations in Gaussian Process Regression. In *ICANN*. Springer, 2011.
- Scheuerer, M. and Schlather, M. Covariance models for divergence-free and curl-free random vector fields. *Stoch. Models*, 2012.
- Solin, A., Kok, M., Wahlström, N., Schön, T. B., and Särkkä, S. Modeling and Interpolation of the Ambient Magnetic Field by Gaussian Processes. *IEEE Transactions on Robotics*, 2018.
- Swain, P. S., Stevenson, K., Leary, A., Montano-Gutierrez, L. F., Clark, I. B., Vogel, J., and Pilizota, T. Inferring time derivatives including cell growth rates using gaussian processes. *Nature communications*, 2016.
- Wahlström, N., Kok, M., Schön, T. B., and Gustafsson, F. Modeling Magnetic Fields using Gaussian Processes. In *Proceedings of the 38th International Conference on Acoustics, Speech, and Signal Processing (ICASSP)*, 2013.

A. Calculation of B-EPGP basis for heat and wave equations

A.1. Dirichlet and Neumann conditions on halfspaces

We will look at systems

$$\begin{cases} A(\partial)u = 0 & \text{in } \mathbb{R}_+^n \\ B(\partial)u = 0 & \text{on } \mathbb{R}^{n-1} \end{cases}$$

where the boundary conditions are Dirichlet ($B = 1$) or Neumann ($B = \partial_n$). These are some of the most common boundary conditions used in PDE. As in the body of our paper, A will be assumed to be a single equation and u a scalar field (in Appendix C we will explain the extension to systems and vector fields). By an affine change of variable, \mathbb{R}_+^n can be replaced with any other halfspace.

Inspired by the Ehrenpreis-Palamodov Theorem 2.1, we will investigate linear combinations of exponential solutions

$$u(x) = \sum_{j=1}^M w_j e^{x \cdot z_j}$$

which satisfy $A(\partial u) = 0$ if

$$\sum_{j=1}^M w_j A(z_j) e^{x \cdot z_j} = 0,$$

which implies $A(z_j) = 0$. This gives our first restriction $z_j \in V = \{z \in \mathbb{C}^n : A(z) = 0\}$, where V is the *characteristic variety* of A . We proceed to incorporate the boundary condition as well. For this, we write $x = (x', x_n)$ and in general z' is the projection of $z \in \mathbb{C}^n$ on \mathbb{C}^{n-1} and $z = (z', z_n)$. We get

$$\sum_{j=1}^M w_j B(z_j) e^{x' \cdot z'_j} = 0,$$

which now does *not* imply $B(z_j) = 0$ since some of the exponentials may be identical, i.e., some $z_j \in V$ may have the same z'_j . Therefore, for each unique z'_j , we will have that

$$\sum_{\{j : z'_j = z'_j\}} w_j B(z_j) = 0.$$

This motivates our definition of the **boundary characteristic variety**

$$V' = \{\zeta \in \mathbb{C}^{n-1} : \zeta = z' \text{ for some } z \in V\},$$

as well as giving the ansatz for the B-EPGP basis

$$\left\{ \sum_{z \in V \text{ s.t. } z' = \zeta} w_z e^{x \cdot z} : \sum_{z \in V \text{ s.t. } z' = \zeta} w_z B(z) = 0 \right\}_{\zeta \in V'}.$$

We simplify this explicitly for Dirichlet and Neumann boundary conditions, first Dirichlet:

$$\left\{ \sum_{z \in V \text{ s.t. } z' = \zeta} w_z e^{x \cdot z} : \sum_{z \in V \text{ s.t. } z' = \zeta} w_z = 0 \right\}_{\zeta \in V'} \quad (7)$$

and then Neumann

$$\left\{ \sum_{z \in V \text{ s.t. } z' = \zeta} w_z e^{x \cdot z} : \sum_{z \in V \text{ s.t. } z' = \zeta} w_z z_n = 0 \right\}_{\zeta \in V'} \quad (8)$$

We will calculate this explicitly for examples in the following.

A.2. Wave equation

We will calculate the B-EPGP bases for Dirichlet and Neumann for the 2-D wave equation in the domain $y > 0$. The calculations extend easily to arbitrary dimensions, but the formulas are cumbersome and we do not include them here. Our calculations extend to all halfspaces parallel to the t -axis by affine changes of variable. Considering boundary conditions on halfspaces that are not parallel to the time axis would violate the physical meaning of initial and boundary conditions.

We start with Dirichlet conditions. To be specific we look at

$$\begin{cases} u_{tt} - (u_{xx} + u_{yy}) = 0 & \text{in } \{(t, x, y) : y > 0\} \\ u = 0 & \text{at } (t, x, 0). \end{cases}$$

In this case,

$$V = \{(a, b, c) \in \mathbb{C}^3 : a^2 = b^2 + c^2\},$$

so $a = \pm\sqrt{b^2 + c^2}$, meaning a can be any complex root of $z^2 - (b^2 + c^2) = 0$. In this case it we have that

$$V' = \mathbb{C}^2,$$

since for any $(a, b) \in \mathbb{C}^2$ there are generically two $c \in \mathbb{C}$ such that $(a, b, c) \in V$.

We proceed with computing the basis for Dirichlet boundary conditions, so we substitute in (7) to get that for any $a, b \in \mathbb{C}$, the vectors $(a, b, c) \in V$ are given by $c = \pm\sqrt{a^2 - b^2}$, so if we write $z^\pm = (a, b, \pm\sqrt{a^2 - b^2})$, the relations in (7) are

$$w_{z^+} + w_{z^-} = 0 \implies w_{z^-} = -w_{z^+},$$

which leads to the basis

$$\{e^{at+bx+\sqrt{a^2-b^2}y} - e^{at+bx-\sqrt{a^2-b^2}y}\}_{a,b \in \mathbb{C}}.$$

This can be rearranged as

$$\{e^{\pm\sqrt{a^2+b^2}t+ax+by} - e^{\pm\sqrt{a^2+b^2}t+ax-by}\}_{a,b \in \mathbb{C}},$$

which is what we have in Example 3.3.

In the case of Neumann boundary conditions, the calculation is similar. Using the same notation for z^\pm as above, we get from (8) that

$$cw_{z^+} - cw_{z^-} = 0 \implies w_{z^-} = w_{z^+},$$

which leads to the basis

$$\{e^{at+bx+\sqrt{a^2-b^2}y} + e^{at+bx-\sqrt{a^2-b^2}y}\}_{a,b \in \mathbb{C}}.$$

This can be rearranged as

$$\{e^{\pm\sqrt{a^2+b^2}t+ax+by} + e^{\pm\sqrt{a^2+b^2}t+ax-by}\}_{a,b \in \mathbb{C}},$$

which is what we have in Example 3.4.

A.3. Heat equation

We will proceed similarly to the previous subsection. The same considerations concerning higher dimensions and choosing various halfspaces apply. We look at

$$\begin{cases} u_t - (u_{xx} + u_{yy}) = 0 & \text{in } \{(t, x, y) : y > 0\} \\ u = 0 & \text{at } (t, x, 0). \end{cases}$$

In this case,

$$V = \{(a, b, c) \in \mathbb{C}^3 : a = b^2 + c^2\},$$

so $a = b^2 + c^2$. In this case it we have that

$$V' = \mathbb{C}^2,$$

since for any $(a, b) \in \mathbb{C}^2$ there are generically two $c \in \mathbb{C}$ such that $(a, b, c) \in V$.

We proceed with computing the basis for Dirichlet boundary conditions, so we substitute in (7) to get that for any $a, b \in \mathbb{C}$, the vectors $(a, b, c) \in V$ are given by $c = \pm\sqrt{a-b^2}$, so if we write $z^\pm = (a, b, \pm\sqrt{a-b^2})$, the relations in (7) are

$$w_{z^+} + w_{z^-} = 0 \implies w_{z^-} = -w_{z^+},$$

which leads to the basis

$$\{e^{at+bx+\sqrt{a-b^2}y} - e^{at+bx-\sqrt{a-b^2}y}\}_{a,b \in \mathbb{C}}.$$

This can be rearranged as

$$\{e^{(a^2+b^2)t+ax+by} - e^{(a^2+b^2)t+ax-by}\}_{a,b \in \mathbb{C}},$$

which is slightly more general than what we have in Example 3.2.

In the case of Neumann boundary conditions, the calculation is similar. Using the same notation for z^\pm as above, we get from (8) that

$$cw_{z^+} - cw_{z^-} = 0 \implies w_{z^-} = w_{z^+},$$

which leads to the basis

$$\{e^{at+bx+\sqrt{a-b^2}y} + e^{at+bx-\sqrt{a-b^2}y}\}_{a,b \in \mathbb{C}}.$$

This can be rearranged as

$$\{e^{(a^2+b^2)t+ax+by} + e^{(a^2+b^2)t+ax-by}\}_{a,b \in \mathbb{C}},$$

which is slightly more general than what we have in Example 3.4 for the 1-D heat equation.

B. Proof that B-EPGP gives all solutions for heat and wave equations

We will prove Theorem 3.5 which applies to heat $\partial_t u - \Delta u = 0$ and wave equations $\partial_t^2 u - \Delta u = 0$ (here we use the notation $\Delta u = \partial_{x_1}^2 + \partial_{x_2}^2 + \dots + \partial_{x_n}^2$ for the Laplacian operator) and any halfspace parallel to the time axis. Since the Laplacian operator is invariant under rotations, we can perform an affine change of variable to reduce the boundary condition to the plane $x_1 = 0$. Our proof below stems from the fact that, in the case of both equations, given a solution in $\{x_1 > 0\}$ with Dirichlet (resp. Neumann) boundary conditions on $\{x_1 = 0\}$, its odd (resp. even) extension with respect to $\{x_1 = 0\}$ will satisfy the same equation in full space.

We will only show the calculations in the case of the 2-D wave equation with Dirichlet boundary condition. Increasing the dimension barely changes the argument. The modification required to deal with the heat equation is also minimal (one less integration by parts in time). To deal with the Neumann boundary condition, one uses even extension instead of odd extension in the calculation.

Proof of Theorem 3.5. Writing $\square u = u_{tt} - u_{xx} - u_{yy}$, we consider smooth solutions of

$$\begin{cases} \square u = 0 & \text{for } x > 0, y \in \mathbb{R}, t > 0 \\ u(t, 0, y) = 0 & \text{for } y \in \mathbb{R}, t > 0. \end{cases}$$

The main observation is that the odd extension (even for Neumann boundary condition) of u is a solution in full space of the wave equation. Let

$$v(t, x, y) = \begin{cases} u(t, x, y) & \text{for } x \geq 0 \\ -u(t, -x, y) & \text{for } x < 0. \end{cases}$$

Clearly $\square v(t, x, y) = 0$ for $x \neq 0$. We still need to check that $\square v = 0$ across $x = 0$, but since the odd extension need not have two classical derivatives, we compute the *distributional derivative* across $x = 0$. To see this let $\phi \in C_c^\infty(\{t > 0\})$ be a test function. We write $dV = dx dy dt$ and integrate by parts

$$\begin{aligned} \int v \square \phi dV &= \int_{x>0} u \square \phi dV - \int_{x<0} u(t, -x, y) \square \phi(t, x, y) dV \\ &= - \int_{x=0} u \phi_x dy dt - \int_{x>0} u_t \phi_t - u_x \phi_x - u_y \phi_y dV \end{aligned}$$

$$\begin{aligned}
 & - \int_{x=0} u \phi_x dy dt + \int_{x<0} u_t(t, -x, y) \phi_t(t, x, y) + u_x(t, -x, y) \phi_x(t, x, y) - u_y(t, -x, y) \phi_y(t, x, y) dV \\
 & = - \int_{x=0} u_x \phi dy dt + \int_{x>0} \phi \square u dV + \int_{x=0} u_x \phi dy dt + \int_{x<0} \phi \square u dV = 0,
 \end{aligned}$$

so indeed $\square v = 0$ in full space. Since v is odd, we have

$$v(t, x, y) = \frac{1}{2}v(t, x, y) - \frac{1}{2}v(y, -x, y),$$

so for $x > 0$ we obtain

$$u(t, x, y) = \frac{1}{2}u(t, x, y) - \frac{1}{2}u(y, -x, y). \quad (9)$$

By Ehrenpreis–Palamodov Theorem 2.1 we know that we can approximate

$$u(t, x, y) \approx \sum_j c_j e^{\alpha_j t + \beta_j x + \gamma_j y}$$

for some $\alpha_j, \beta_j, \gamma_j \in \mathbb{C}$ with $\alpha_j^2 = \beta_j^2 + \gamma_j^2$. By (9), it follows that

$$u(t, x, y) \approx \sum_j \frac{1}{2} c_j (e^{\alpha_j t + \beta_j x + \gamma_j y} - e^{\alpha_j t - \beta_j x + \gamma_j y}).$$

This is exactly the basis produced by our B-EPGP algorithm, see Example 3.3. \square

We next look at the heat and wave equation in rectangles and give a generalization of Theorems 3.8 and 3.10:

Theorem B.1 (Heat and Wave in rectangles). *Let $A = \partial_t - \Delta$ or $A = \partial_{tt}^2 u - \Delta u$, $\Omega = [0, L_1] \times [0, L_2] \times \dots \times [0, L_n]$, and B be Dirichlet or Neumann boundary condition on $\partial\Omega \times \mathbb{R}$. Consider the equation*

$$\begin{cases} Au = 0 & \text{in } \Omega \times \mathbb{R} \\ Bu = 0 & \text{on } \partial\Omega \times \mathbb{R}. \end{cases}$$

Then B-EPGP gives the basis with dense linear span

$$\{e^{\sqrt{-1}ht} f(j_1 x_1 \pi / L_1) f(j_2 x_2 \pi / L_2) \dots f(j_n x_n \pi / L_n) : j_1, j_2, \dots, j_n \in \mathbb{Z}\},$$

where

- $h = j_1^2 + j_2^2 + \dots + j_n^2$ for heat equation and $h = \pm \sqrt{j_1^2 + j_2^2 + \dots + j_n^2}$ for wave equation,
- $f = \sin$ for Dirichlet boundary condition and $f = \cos$ for Neumann boundary condition.

Proof. We will only cover the case of the wave equation with Dirichlet boundary conditions. We will make some simplifications which do not restrict the idea of proof: we set $n = 2$ so $u = u(t, x, y)$ and $L_1 = L_2 = \dots = L_n = \pi$.

Let u be a solution of

$$\begin{cases} \square u = 0 & \text{for } x \in (0, \pi), y \in (0, \pi) \\ u = 0 & \text{for } x \text{ or } y = 0 \text{ or } \pi. \end{cases}$$

We define the extension to $x, y \in (0, 2\pi)$ by

$$v(t, x, y) = \begin{cases} u(t, x, y) & x \in (0, \pi), y \in (0, \pi) \\ -u(t, x - \pi, y) & x \in (\pi, 2\pi), y \in (0, \pi) \\ -u(t, x, y - \pi) & x \in (0, \pi), y \in (\pi, 2\pi) \\ u(t, x - \pi, y - \pi) & x \in (\pi, 2\pi), y \in (\pi, 2\pi). \end{cases}$$

We extend v by periodically in (x, y) with cell $(0, 2\pi)^2$ to \mathbb{R}^{1+2} without changing its name. We make several observations:

- For each t , the function $(x, y) \mapsto v(t, x, y)$ is $(0, 2\pi)^2$ -periodic, therefore v has a Fourier expansion $\sum_{j,k \in \mathbb{Z}} f_{j,k}(t) e^{i(jx+ky)}$.
- For each (t, x) , the function $y \mapsto v(t, x, y)$ is odd, therefore only the terms $\sin(ky)$ will appear in the Fourier expansion.
- Similarly $x \mapsto v(t, x, y)$ is odd, so v has a Fourier expansion $\sum_{j,k \in \mathbb{Z}} f_{j,k}(t) \sin(jx) \sin(ky)$.
- v solves the equation in full space, $\square v = 0$ in \mathbb{R}^{1+2} .

Only the last assertion is non-obvious and requires a careful distributional calculation as in the proof of Theorem 3.5 above, taking $\phi \in C_c^\infty(\mathbb{R}^{1+2})$ and showing that $\int u \square \phi dV = 0$ by careful integration by parts. We omit the details.

Finally, we plug in $v = \sum_{j,k \in \mathbb{Z}} f_{j,k}(t) \sin(jx) \sin(ky)$ in the equation $\square v = 0$ to obtain $f_{j,k}''(t) + (j^2 + k^2) f_{j,k}(t) = 0$, which is an ODE with linearly independent solutions $e^{\pm\sqrt{-1}\sqrt{j^2+k^2}t}$. This gives us the Fourier basis

$$e^{\pm\sqrt{-1}\sqrt{j^2+k^2}t} \sin(jx) \sin(ky) \quad \text{for } j, k \in \mathbb{Z},$$

which is the basis computed using B-EPGP in Example 3.9. This coincides with the *separation of variables* method. \square

The same extension works for the heat equation with Dirichlet boundary condition. For the Neumann boundary condition (for both equations), one removes the two “minus” signs in rows 2 and 3 of the definition of v ; its periodic extension is thus an even function. Higher dimensions take more effort to set up v on 2^n branches, but the idea is the same.

C. Ehrenpreis–Palamodov Theorem and EPGP

We will begin with a very precise version of the statement that *exponential-polynomial solutions are dense in the space of all solutions* for a linear PDE system.

Theorem C.1. *Let $R = \mathbb{C}[\partial]$ and $\Omega \subset \mathbb{R}^n$ be an open convex set. Let $A \in R^{\ell \times k}$ and $V = \{z \in \mathbb{C}^n : \ker A(z) \neq 0\}$. Then there exist a decomposition $V = \bigcup_{i=1}^m V_i$ into irreducible varieties V_i and a set of vector polynomials in $2n$ variables called Noetherian multipliers $\{p_{i,j}\}_{j=1, \dots, r_i, i=1, \dots, m} \subset \mathbb{C}[x, z]^k$ such that solutions of the form*

$$\sum_{h=1}^N \sum_{i=1}^m \sum_{j=1}^{r_i} c_{i,j,h} p_{i,j}(x, z_{i,j,h}) e^{x \cdot z_{i,j,h}} \quad \text{with } z_{i,j,h} \in V_i \quad (\text{EP})$$

are dense in the space of smooth solutions of $A(\partial)u(x) = 0$ in Ω .

Next, we clarify the notion of smooth solution and the topology with respect to which we have density. First, we write $\mathcal{F} = C^\infty(\Omega)$ to be the space of smooth functions $\Omega \rightarrow \mathbb{C}$. This is a Fréchet space under the standard topology induced by the semi-norms $s_{a,b}(u) = \max_{|\alpha|=a, x \in \Omega_b} |\partial^\alpha u(x)|$, where $\Omega_b \uparrow \Omega$ is an increasing sequence of compact sets which exhausts Ω . This is to say that a sequence $u_q \rightarrow u$ in \mathcal{F} if $s_{a,b}(u_q - u) \rightarrow 0$ for all a, b . Algebraically, \mathcal{F}^k is an R -module under the action of differentiation.

Our solution space is then

$$\ker_{\mathcal{F}} A = \{u \in \mathcal{F}^k : A(\partial)u = 0\}.$$

Ehrenpreis–Palamodov Theorem states that each element $u \in \ker_{\mathcal{F}} A$ can be approximated by $u_q \rightarrow u$ in \mathcal{F}^k with solutions u_q of the form (EP).

Our earlier algorithm EPGP from (Harkonen et al., 2023) revolves around fitting coefficients $c_{i,j,h}$ and “frequencies” $z_{i,j,h}$ in formula (EP). To simplify notation, we will simply write $\{b(x; z)\}_{z \in V}$ for the continuously indexed basis that we are working with (exponential-polynomial solutions of $A(\partial)u = 0$). We will write our predictions in form

$$\phi(x) = \sum_{j=1}^N c_j b(x; z_j). \quad (10)$$

We will assume that our solution is given as data points $y_h \approx u(x_h)$ for $h = 1, \dots, M$, where $N \ll M$. We write $C = (c_j) \in \mathbb{C}^N$, $Z = (z_j) \in V^N$, $X = (x_h) \in \mathbb{R}^M$, $Y = (y_h) \in \mathbb{C}^M$.

We will model $C \sim \mathcal{N}(0, \Sigma)$ as multivariate Gaussian distribution with covariance $\Sigma = \text{diag}(\sigma_j^2)_{j=1}^N$. We will also assume that the data has Gaussian noise, so $Y - \phi(X) \sim \mathcal{N}(0, \sigma_0^2 I_M)$. Writing $B = (b(x_h; z_j)) \in \mathbb{C}^{M \times N}$, we have that $\phi(X) = BC$, so $\phi(X) \sim \mathcal{N}(0, B\Sigma B^T)$. We write $\sigma^2 = (\sigma_j^2)_{j=0}^N$ for the vector of parameters of the underlined distributions. The marginal log likelihood for this model is maximized if the function

$$L(Z, \sigma^2; X, Y) = \frac{1}{\sigma_0^2} (|Y|^2 - Y^H B A^{-1} B^H Y) + (M - N) \log \sigma_0^2 + \log \det \Sigma + \log \det A,$$

is minimized, where $A = N\sigma_0^2 \Sigma^{-1} + B^H B$ and H denotes the conjugate-transpose operation. We then use stochastic gradient descent to minimize $L(Z, \sigma^2)$. Once we obtain Z , we plug in the explicit formula for $C = A^{-1} B^H Y$ and use (10) as our prediction.

D. Free wave equation in 2D and 3D

In fact, our first improvement of EPGP is to update it to include initial speeds as well as initial conditions. We will explain this for the example of the wave equation in arbitrary dimension n .

Even without boundary conditions, this is an important example for which ongoing research is being developed (Henderson et al., 2023). Writing $\square u = u_{tt} - u_{x_1 x_1} - u_{x_2 x_2} - \dots - u_{x_n x_n}$, the problem to consider is the **Free Wave Equation**:

$$\begin{cases} \square u = 0 & \text{in } \mathbb{R}^n \times (0, \infty) \\ u(0, x) = f(x) & \text{for } x \in \mathbb{R}^n \\ u_t(0, x) = g(x) & \text{for } x \in \mathbb{R}^n. \end{cases}$$

Vanilla EPGP only deals with the case $g = 0$. Our main observation is that if u is a GP solution with covariance kernel k , then (u, u_t) is a GP with covariance kernel

$$\begin{bmatrix} k(x, t; x', t') & \partial_t k(x, t; x', t') \\ \partial_{t'} k(x, t; x', t') & \partial_{t'}^2 k(x, t; x', t') \end{bmatrix}$$

which we fit to data $(u(0, X), u_t(0, X)) = (f(X), g(X))$. Mathematically, this is the same as considering the PDE system

$$\begin{cases} \square u = 0 & \text{in } \mathbb{R}^n \times (0, \infty) \\ v - u_t = 0 & \text{in } \mathbb{R}^n \times (0, \infty) \\ u(0, x) = f(x) & \text{for } x \in \mathbb{R}^n \\ v(0, x) = g(x) & \text{for } x \in \mathbb{R}^n. \end{cases}$$

This can then be solved using Vanilla EPGP for $A(u, v) = (\square u, v - u_t)$ with initial condition for both u and v .

As an example, we will consider the two dimensional case,

$$\begin{cases} u_{tt} = u_{xx} + u_{yy} & \text{in } \mathbb{R}^2 \times (0, \infty) \\ u(0, x, y) = f(x - 2) + f(y - 2) & \text{in } \mathbb{R}^2 \\ u_t(0, x, y) = f'(x - 2) + f'(y - 2) & \text{in } \mathbb{R}^2, \end{cases}$$

where $f(x) = \exp(-5x^2)$ or $f(x) = \cos(5x)$. The true solution is given by $u(t, x, y) = f(x + t - 2) + f(y + t - 2)$ and our results can be found in Figure 9.

E. Check using conservation of energy

So far, we checked the accuracy of our results either by comparison with true solutions (wherever we could construct them) or by comparison with other solvers. For certain equations, there is another mathematical tool that we can use, namely conservation of energy:

Theorem E.1. *Let $\Omega \subset \mathbb{R}^d$ be a convex, bounded, open set and consider a smooth solution $u \in C^\infty(\bar{\Omega} \times [0, \infty))$ of the wave equation*

$$\square u = 0 \quad \text{in } \Omega \times (0, \infty).$$

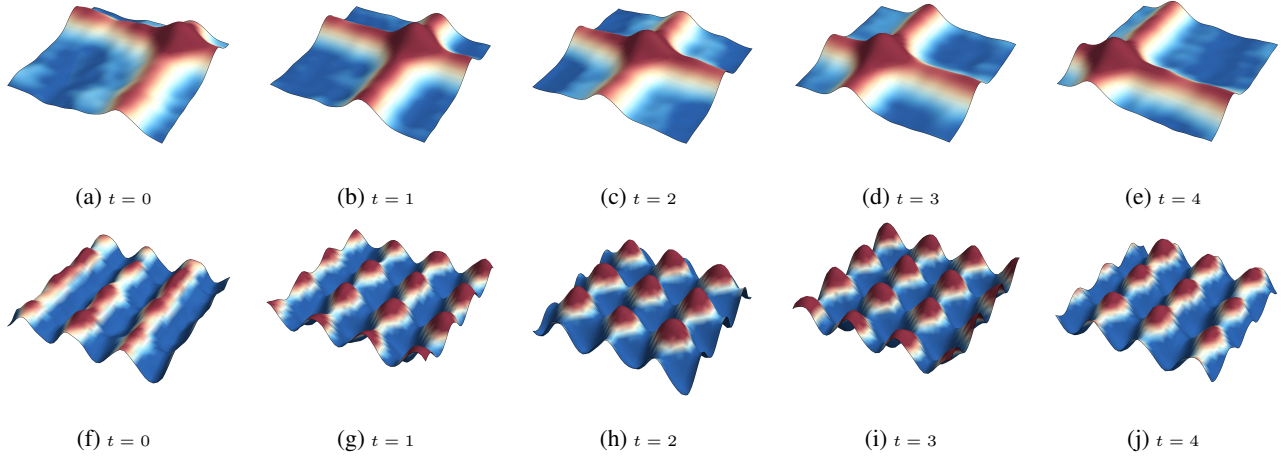


Figure 9: Solutions to the initial boundary value problem for the 2-D wave equation (no boundary conditions). Solution fits both initial condition and initial speed. This is a necessary improvement of the EPGP algorithm from (Harkonen et al., 2023), which can produce non-physical solutions in certain cases. Animations can be found in the ancillary files `exp_free.mp4` and `cos_free.mp4`.

Suppose that u satisfies Dirichlet or Neumann boundary conditions

$$u = 0 \quad \text{or} \quad \frac{\partial u}{\partial n} = 0 \quad \text{for } x \in \partial\Omega.$$

Then the **energy** of the solution u

$$E(t) = \int_{\Omega} \left| \frac{\partial u(x, t)}{\partial t} \right|^2 + \sum_{j=1}^d \int_{\Omega} \left| \frac{\partial u(x, t)}{\partial x_j} \right|^2 dx$$

is constant for all $t \geq 0$.

Proof. We can see that

$$E(t) = \int_{\Omega} u_t^2 + |\nabla u|^2 dx$$

Then we can integrate by parts to obtain

$$\begin{aligned} E'(t) &= \int_{\Omega} [2u_t u_{tt} + 2(\nabla u \cdot \nabla u_t)] dx \\ &= \int_{\Omega} 2u_t u_{tt} dx - 2 \int_{\Omega} (\Delta u) u_t dx + 2 \int_{\partial\Omega} u_t \frac{\partial u}{\partial n} dS \\ &= \int_{\Omega} 2u_t (u_{tt} - \Delta u) dx + 2 \int_{\partial\Omega} u_t \frac{\partial u}{\partial n} dS \\ &= 2 \int_{\partial\Omega} u_t \frac{\partial u}{\partial n} dS. \end{aligned}$$

For either Dirichlet or Neumann boundary condition, we have that

$$\int_{\partial\Omega} u_t \frac{\partial u}{\partial n} dS = 0,$$

Therefore, $E(t)$ is indeed constant. □

In practice, we approximate $E(t)$ a Riemann sum of step-size h . For instance, when $d = 2$ we take

$$Q(t) = \frac{\text{Area}(\Omega)}{\#(h\mathbb{Z})^2 \cap \Omega} \sum_{(x,y) \in (h\mathbb{Z})^2 \cap \Omega} (u_t^2 + u_x^2 + u_y^2)|_{(x,y,t)}.$$

The quantity we implement in our code is

$$\tilde{Q}(hT) = \sum_{(x,y) \in (h\mathbb{Z})^2 \cap \Omega} (u_t^2 + u_x^2 + u_y^2)|_{(x,y,hT)} \quad (11)$$

where T is the final time ($t \in [0, T]$) and we choose $h = .1$.

F. Wave equation in bounded domains

In this section we will provide numerical results for the 2-D wave equation in bounded domains, meaning that we investigate $u_{tt} - (u_{xx} + u_{yy}) = 0$ in $\Omega \times (0, T)$ with Dirichlet or Neumann boundary conditions on $\partial\Omega$, where $\Omega \subset \mathbb{R}^2$ will be a bounded open convex set. We will use both EPGP (Section 3.1) and B-EPGP methods and compare them.

We will check the validity of our results using the conservation of energy principle from Theorem E.1. We will show that by using EPGP a non-negligible amount of energy is lost/dissipated. In fact, we can say more: We will solve initial boundary value problems with given initial condition and zero initial speed, meaning that we will solve

$$\begin{cases} u_{tt} - (u_{xx} + u_{yy}) = 0 & \text{in } \Omega \times (0, T) \\ u(0, x, y) = f(x, y) & \text{at } t = 0 \\ u_t(0, x, y) = 0 & \text{at } t = 0 \end{cases}$$

which is a well-posed problem under Dirichlet or Neumann boundary conditions. By Theorem E.1 we have

$$E(t) = E(0) = \int_{\Omega} u_t^2(0, x, y) + u_x^2(0, x, y) + u_y^2(0, x, y) dx dy = \int_{\Omega} f_x^2 + f_y^2 dx dy.$$

Thus in our experiments we will compare the energy of the B-EPGP with the true value computed from initial conditions above and also show its superiority to EPGP.

F.1. Rectangular domains

We first consider $\Omega = (0, 4)^2$ and $t \in (0, 12)$ and look for the solution of the initial boundary value problem

$$\begin{cases} u_{tt} - (u_{xx} + u_{yy}) = 0 & \text{for } x, y \in (0, 4), t \in (0, 12) \\ u(0, x, y) = \exp(-10((x-1)^2 + (y-1)^2)) & \text{for } x, y \in (0, 4) \\ u_t(0, x, y) = 0 & \text{for } x, y \in (0, 4) \\ u(t, x, y) = 0 & \text{for } x \text{ or } y = 0 \text{ or } 4. \end{cases}$$

We will give a shortcut to our B-EPGP algorithm for finding a basis. We consider $H_1 = \{x = 0\}$, $H_2 = \{y = 0\}$, $H_3 = \{x = 4\}$, $H_4 = \{y = 4\}$ and let $e^{at+bx+cy}$ be a solution of the wave equation, meaning that $a^2 = b^2 + c^2$. We can calculate a basis for the wedge $\{x, y > 0\}$, see Appendix G.2, which is

$$\begin{aligned} e^{at+bx+cy} - e^{at-bx+cy} - e^{at+bx-cy} + e^{at-bx-cy} &= e^{at}(e^{bx+cy} - e^{-bx+cy} - e^{bx-cy} + e^{-bx-cy}) \\ &= e^{at}(e^{cy}(e^{bx} - e^{-bx}) - e^{-cy}(e^{bx} - e^{-bx})) \\ &= 2\sqrt{-1}e^{at} \sin(bx)(e^{cy} - e^{-cy}) = -4e^{at} \sin(bx) \sin(cy) \end{aligned}$$

Here we observe a shortcut: if we set $b, c \in \mathbb{Z}$, we obtain a set of functions $\{e^{\pm \frac{\pi\sqrt{-1}}{4} \sqrt{j^2+k^2} t} \sin(\frac{\pi}{4} jx) \sin(\frac{\pi}{4} ky)\}_{j,k \in \mathbb{Z}}$ which satisfy the boundary condition on H_2 as well (see also Appendix G.1). That set of functions has linear span which is dense in the set of all solutions to (12) by Theorem B.1.

Snapshots of our solution are presented in Figure 10 and the conservation of energy is demonstrated in Figure 11.

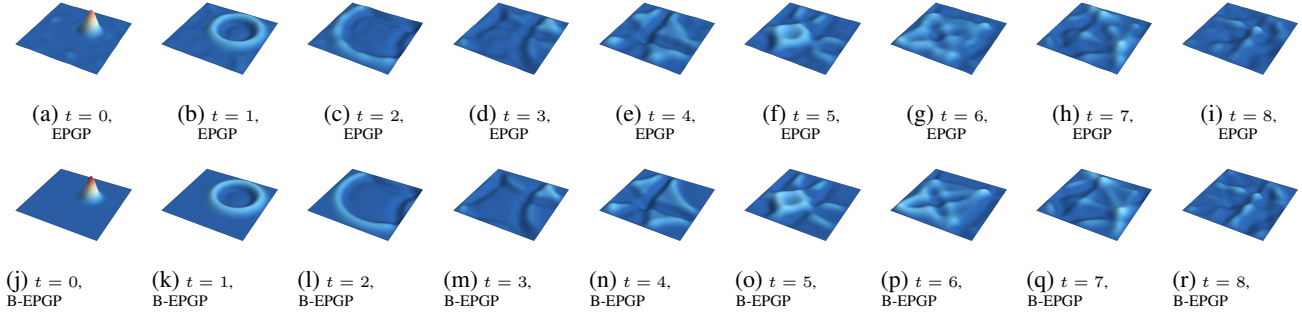


Figure 10: Solution of 2-D wave equation in a rectangular domain calculated using the EPGP and B-EPGP methods. We use a Dirichlet boundary condition which is visible above from the fact that the edges of our plots have the same color in all snapshots. Animations can be found in the ancillary files `rec-S.mp4` and `rec-R.mp4`.

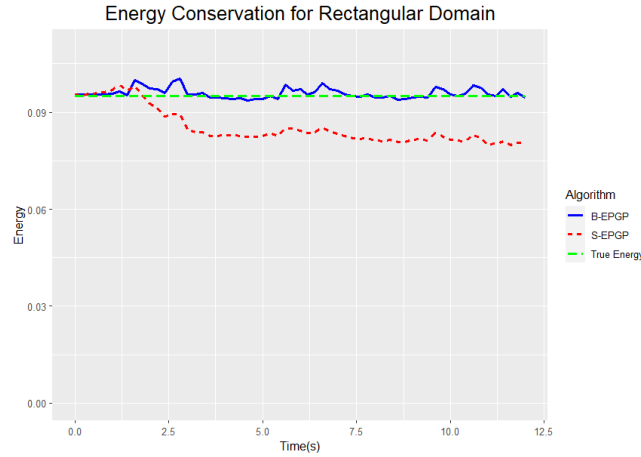


Figure 11: Proof of energy conservation for the 2-D wave equation in a rectangular domain. EPGP method incurs a non-negligible loss of energy. The error in B-EPGP is partly due to our approximation of the energy integral in (11).

F.2. Triangular domains

We next consider $\Omega = \{(x, y) : 0 < y < x < 4\}$ and $t \in (0, 4)$ and look for the solution of the initial boundary value problem

$$\begin{cases} u_{tt} - (u_{xx} + u_{yy}) = 0 & \text{in } \Omega \times (0, 4) \\ u(0, x, y) = \exp(-10((x-3)^2 + (y-3)^2)) & \text{in } \Omega \\ u_t(0, x, y) = 0 & \text{in } \Omega \\ u(t, x, y) = 0 & \text{for } (x, y) \in \partial\Omega \end{cases}$$

We will use the B-EPGP basis computed in Section F.1 and an odd reflection in the diagonal line $y = x$ which gives

$$\left\{ e^{\pm \frac{\pi\sqrt{-1}}{4} \sqrt{j^2+k^2}t} \left[\sin\left(\frac{\pi}{4}jx\right) \sin\left(\frac{\pi}{4}ky\right) - \sin\left(\frac{\pi}{4}kx\right) \sin\left(\frac{\pi}{4}jy\right) \right] \right\}_{j,k \in \mathbb{Z}}.$$

It is easy to see that this new basis satisfies the Dirichlet boundary condition on all three boundary hyperplanes $\{x = 4\}$, $\{y = 0\}$, $\{x = y\}$. Snapshots of our solution are presented in Figure 12 and the conservation of energy is demonstrated in Figure 13.

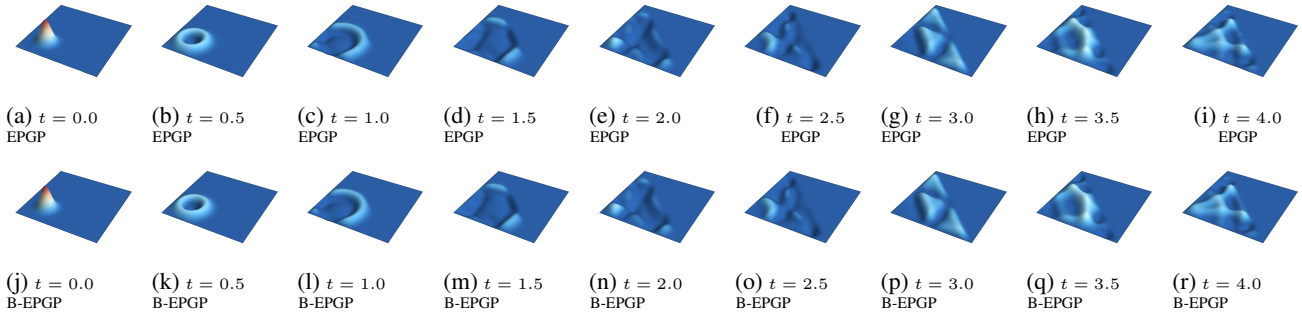


Figure 12: Solution of 2-D wave equation in a triangular domain with Dirichlet boundary conditions calculated using the EPGP and B-EPGP methods. Animations can be found in the ancillary files `triangle.mp4` and `triangleEPGP.mp4`.
Energy Conservation for Triangle Domain

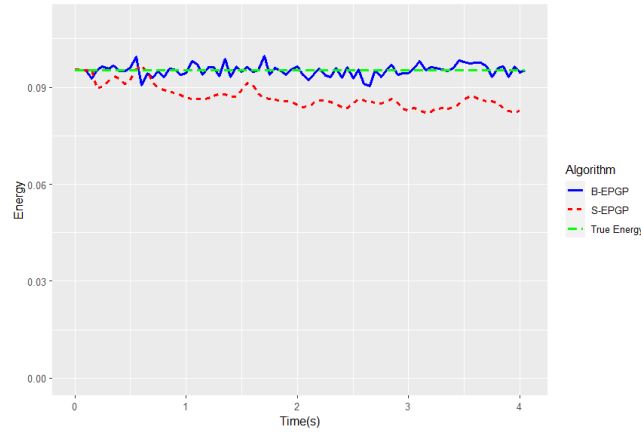


Figure 13: Proof of energy conservation for the 2-D wave equation in a triangular domain. S-EPGP method incurs a non-negligible loss of energy. The error in B-EPGP is partly due to our approximation of the energy integral in (11).

F.3. Circle: Drum membrane

Our methods extend to non polygonal domains. Here we use the direct method from Section 3.1 to cover the 2-D wave equation in a disc, a classic model for circular drum membranes. We will consider $\Omega = \{(x, y) : x^2 + y^2 \leq 16\}$ and $t \in (0, 7)$, and the equations are

$$\begin{cases} u_{tt} - (u_{xx} + u_{yy}) = 0 & \text{in } (0, 7) \times \Omega \\ u(0, x, y) = \exp(-10(x^2 + y^2)) & \text{in } \Omega \\ u_t(0, x, y) = 0 & \text{in } \Omega \\ u(t, x, y) = 0 & \text{on } (0, 7) \times \partial\Omega. \end{cases}$$

Snapshots of our solution are presented in Figure 14 and the conservation of energy is demonstrated in Figure 15.

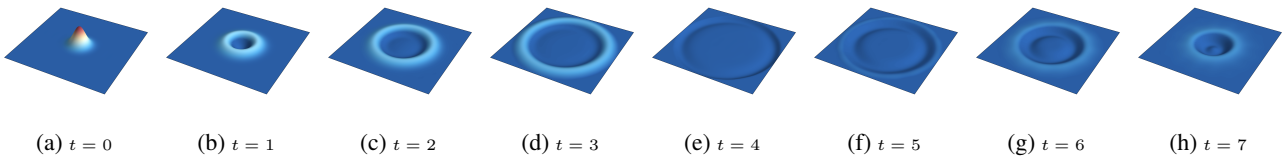


Figure 14: Radially symmetric solution to 2-D wave equation in a circular domain with Dirichlet boundary conditions evaluated at 8 timepoints. The animation can be found in the ancillary file `circle.mp4`.

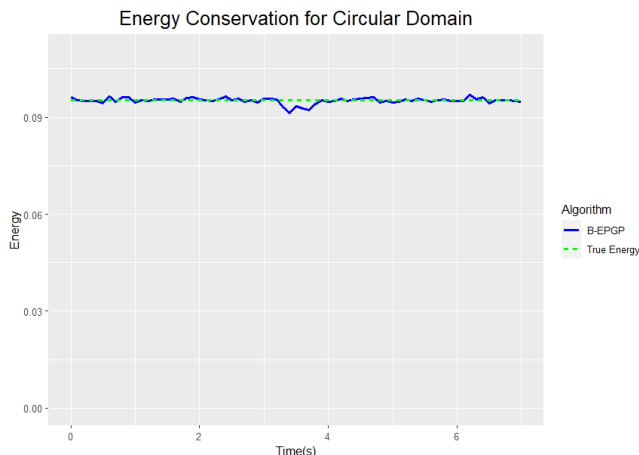


Figure 15: Proof of energy conservation for the 2-D wave equation in a circular domain. The error is partly due to our numerical approximation of the energy integral in (11).

G. B-EPGP bases for wave equation in intersections of two halfspaces

We will also analyze the next simplest case which is more general than halfspaces (Appendix A), namely intersections of two halfspaces. These, have only two relative positions, parallel or not. When the boundary hyperplanes intersect, we will distinguish between the case when the angle is acute or not.

G.1. Parallel halfspaces: slabs

Consider the equation in Example 3.7, namely 1-D wave equation in an interval:

$$\begin{cases} u_{tt} = u_{xx} & x \in (0, \pi), t \in \mathbb{R} \\ u(0, t) = u(\pi, t) = 0 & t \in \mathbb{R}. \end{cases} \quad (12)$$

We will show how to use our B-EPGP algorithm to calculate a basis. We consider $H_1 = \{x = 0\}$, $H_2 = \{x = \pi\}$ and let e^{at+bx} be a solution of the wave equation, meaning that $a^2 = b^2$, so we will simply write $a = \pm b$. We obtain $e^{b(\pm t+x)}$. Using Section A, this basis is extended to a basis which satisfies the H_1 condition by

$$e^{b(\pm t+x)} - e^{b(\pm t-x)} = e^{\pm bt}(e^{bx} - e^{-bx}) = 2e^{\pm bt} \sinh(bx).$$

Here we observe a shortcut: if we set $b \in \sqrt{-1}\mathbb{Z}$, we obtain a set of functions $\{e^{\pm\sqrt{-1}jt} \sin(jx)\}_{j \in \mathbb{Z}}$ which satisfy the boundary condition on H_2 as well. This set has linear span which is dense in the set of all solutions to (12) by Theorem B.1.

A similar calculation gives the basis $\{e^{\pm\sqrt{-1}jt} \cos(jx)\}_{j \in \mathbb{Z}}$ in the case of Neumann boundary conditions $u_x = 0$.

We present our solution to the initial boundary value problem (12) computed using the B-EPGP basis above in Figure 16.

G.2. Large wedges

We will consider the case when the two halfspaces make an angle of 90° (see Example 3.6) and calculate the basis for

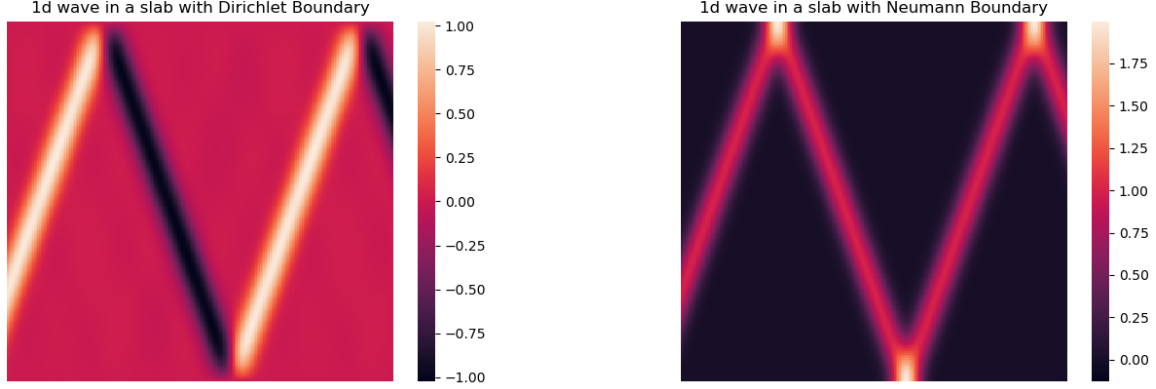
$$\begin{cases} \square u(x, y, t) = 0 & (x, y) \in (0, \infty)^2 \\ u(0, y, t) = 0 & y \in (0, \infty) \\ u_y(x, 0, t) = 0 & x \in (0, \infty). \end{cases}$$

We will calculate our **B-EPGP algorithm** and show the calculations in some detail.

In Step 1 we notice that the boundary hyperplanes are $H_1 = \{x = 0\}$ and $H_2 = \{y = 0\}$.

In Step 2, we begin with one exponential solution

$$e^{at+bx+cy} \quad \text{with } a^2 = b^2 + c^2.$$



(a) Dirichlet boundary condition

(b) Neumann boundary condition

Figure 16: B-EPGP solution for 1-D wave in an infinite slab with different boundary conditions. The difference color is explained by the different reflections: For Dirichlet, a negative wave is reflected (“hard boundary”) and for Neumann a positive wave is reflected (“soft boundary”). This behavior is already readable from the bases calculated in Appendix G.1.

This is extended to a basis that satisfies the H_1 condition by

$$e^{at+bx+cy} - e^{at-bx+cy}.$$

This follows from the calculations in Section A.2. Similarly, we extend to a basis that satisfies the H_2 condition

$$e^{at+bx+cy} + e^{at+bx-cy}.$$

This gives us the intermediate “basis”, at the end of Step 2,

$$b(z) = \{e^{at+bx+cy} - e^{at-bx+cy}, e^{at+bx+cy} + e^{at+bx-cy} : a^2 + b^2 = c^2\}.$$

We proceed with Step 3 and check the both boundary conditions. We notice that each type of basis element satisfies exactly one of the two boundary conditions, so we must return to Step 2.

To extend the term $e^{at+bx+cy} - e^{at-bx+cy}$ (which satisfies the H_1 condition) to satisfy the H_2 condition, we use the same calculation as above to obtain

$$e^{at+bx+cy} - e^{at-bx+cy} + (e^{at+bx-cy} - e^{at-bx-cy}).$$

To extend the term $e^{at+bx+cy} + e^{at+bx-cy}$ (which satisfies the H_2 condition) to satisfy the H_1 condition, we get

$$e^{at+bx+cy} + e^{at+bx-cy} - (e^{at-bx+cy} + e^{at-bx-cy}).$$

Coincidentally, both basis elements constructed above equal

$$e^{at+bx+cy} - e^{at-bx+cy} + e^{at+bx-cy} - e^{at-bx-cy} \quad \text{for } a^2 = b^2 + c^2, \quad (13)$$

which can easily be seen to satisfy both boundary conditions. In particular, we obtain that the algorithm terminates. Thus we obtained the basis claimed in Example 3.6.

G.3. Small wedges

We will also consider and also implement the case of an acute wedge, e.g. $\Omega = \{(x, y) : x > 0, y < x\}$ and $t \in (0, 8)$. We will look at the 2-D wave equation with Neumann boundary conditions

$$\begin{cases} u_{tt} - (u_{xx} + u_{yy}) = 0 & \text{in } \Omega \times (0, 8) \\ u(0, x, y) = \exp(-10((x-3)^2 + (y-1)^2)) & \text{in } \Omega \\ u_t(0, x, y) = 0 & \text{in } \Omega \\ u_n(t, x, y) = 0 & \text{on } \partial\Omega \times (0, 8). \end{cases}$$

The B-EPGP basis can be computed along the same lines as the case of the right angle above. However, the calculations are much more ample so we only state the result here:

$$\begin{aligned}
 & e^{z_1x+z_2y+\tau t} + e^{-z_1x+z_2y+\tau t} + e^{z_1x-z_2y+\tau t} + e^{-z_1x-z_2y+\tau t} \\
 & + e^{z_2x+z_1y+\tau t} + e^{-z_2x+z_1y+\tau t} + e^{z_2x-z_1y+\tau t} + e^{-z_2x-z_1y+\tau t} \\
 & + e^{z_1x+z_2y-\tau t} + e^{-z_1x+z_2y-\tau t} + e^{z_1x-z_2y-\tau t} + e^{-z_1x-z_2y-\tau t} \\
 & + e^{z_2x+z_1y-\tau t} + e^{-z_2x+z_1y-\tau t} + e^{z_2x-z_1y-\tau t} + e^{-z_2x-z_1y-\tau t} \quad \text{for } \tau^2 = z_1^2 + z_2^2.
 \end{aligned}$$

We present our solution to the initial boundary value problem computed using the B-EPGP basis above in Figure 17.

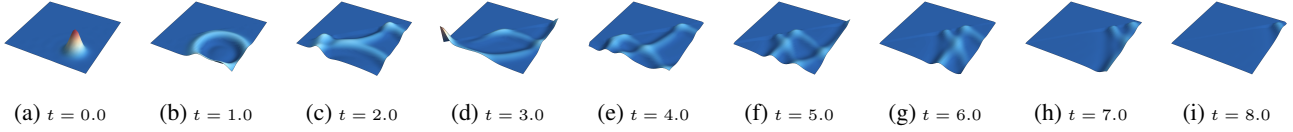


Figure 17: Solution of 2-D wave equation in a 45° wedge domain evaluated at 9 timepoints. Since the domain is unbounded, the wave leaves the domain in finite time. The animation can be found in the ancillary file `goodwedge.mp4`.

H. Heat equation in 2-D

The examples we gave so far focused on wave equations, often in 2 space dimensions as these produce the most visually striking videos and are better represented in the paper as snapshots at various times. Our method extends equally well to equations for heat, which we will give an example of in this section. We will consider a wedge domain and Neumann boundary conditions:

$$\begin{cases}
 u_t - (u_{xx} + u_{yy}) = 0 & \text{in } (0, 4) \times (0, \infty)^2 \\
 u(0, x, y) = 5 \exp(-10((x-1)^2 + (y-1)^2)) & \text{in } (0, \infty)^2 \\
 u_x(t, 0, y) = 0 & \text{for } t \in (0, 4), y \in (0, \infty) \\
 u_y(t, x, 0) = 0 & \text{for } t \in (0, 4), x \in (0, \infty).
 \end{cases}$$

In this case, we can use the calculations in Section A.3 and G.2 to obtain the B-EPGP basis

$$e^{(a^2+b^2)t+ax+by} + e^{(a^2+b^2)t-ax+by} + e^{(a^2+b^2)t+ax-by} + e^{(a^2+b^2)t-ax-by} \quad \text{for } a, b \in \mathbb{C}.$$

For comparison, we will also consider the case of Dirichlet boundary conditions

$$\begin{cases}
 u_t - (u_{xx} + u_{yy}) = 0 & \text{in } (0, 4) \times (0, \infty)^2 \\
 u(0, x, y) = 5 \exp(-10((x-1)^2 + (y-1)^2)) & \text{in } (0, \infty)^2 \\
 u(t, 0, y) = 0 & \text{for } t \in (0, 4), y \in (0, \infty) \\
 u(t, x, 0) = 0 & \text{for } t \in (0, 4), x \in (0, \infty),
 \end{cases}$$

for which we obtain the B-EPGP basis

$$e^{(a^2+b^2)t+ax+by} - e^{(a^2+b^2)t-ax+by} - e^{(a^2+b^2)t+ax-by} + e^{(a^2+b^2)t-ax-by} \quad \text{for } a, b \in \mathbb{C}.$$

In Figure 18 we will further compare these results visually with the solution of the heat equation in full space

$$\begin{cases}
 u_t - (u_{xx} + u_{yy}) = 0 & \text{in } (0, 4) \times \mathbb{R}^2 \\
 u(0, x, y) = 5 \exp(-10((x-1)^2 + (y-1)^2)) & \text{in } \mathbb{R}^2.
 \end{cases}$$

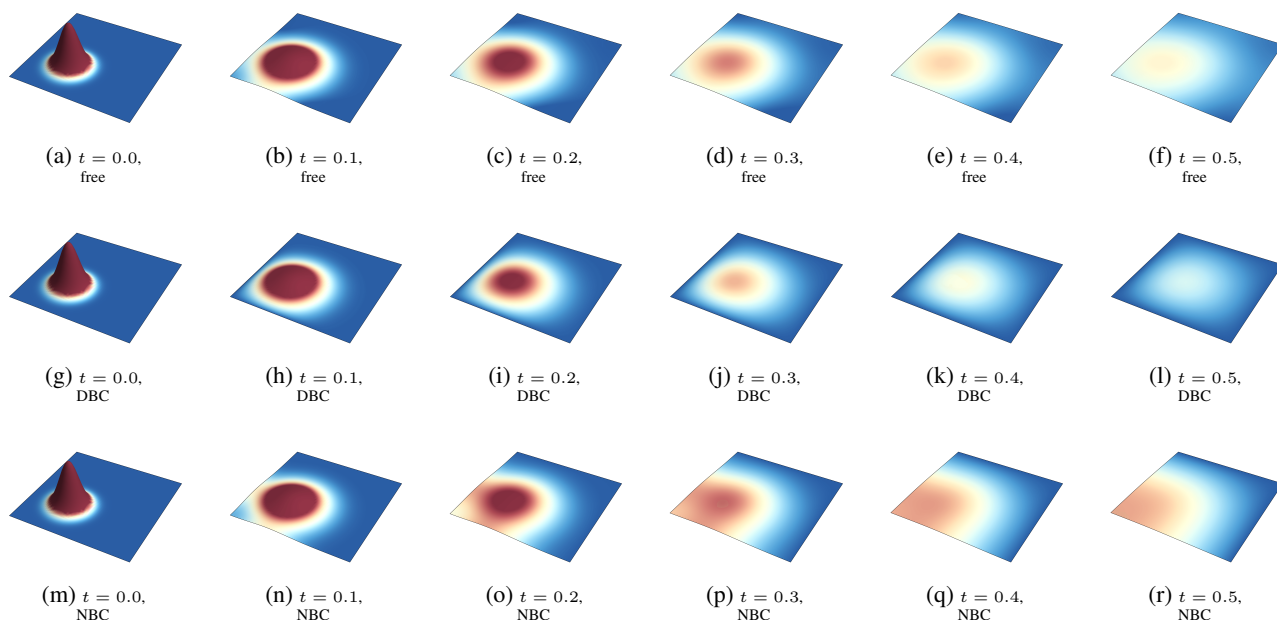


Figure 18: Snapshots of our solution for 2-D heat equation with different boundary condition at 6 timepoints. The effects of the boundary conditions are very clearly visible. Row 1, free heat equation (no BC): heat diffuses exponentially in time. Row 2, Dirichlet BC: heat is maintained at 0 on the edges $x = 0$ and $y = 0$ so heat is diffused faster. Row 3, Neumann BC: the edges $x = 0$ and $y = 0$ are thermally insulated, so no heat is diffused there; hence heat is diffused slower, in directions of large x, y . Animations can be found in the ancillary files `heatNBC.mp4`, `heatDBC.mp4` and `freeheat.mp4`.

I. Laplace Equation which has a singular point

By its very ansatz, EPGP produces global solutions, since each exponential-polynomial solution is a solution in full space (see also Appendix C). Here we demonstrate that our methods can approximate solutions on bounded domains Ω which cannot be extended to a global solution on \mathbb{R}^n . This somewhat surprising fact shows that B-EPGP approximates solutions *locally* very well.

Let $\Omega \subset \mathbb{R}^2$ be such that $0 \notin \bar{\Omega}$. We consider the problem

$$\begin{cases} u_{xx} + u_{yy} = 0 & \text{in } \Omega \\ u = \log(x^2 + y^2) & \text{for } (x, y) \in \partial\Omega. \end{cases}$$

For this boundary condition, there is no v satisfying $v_{xx} + v_{yy} = 0$ in \mathbb{R}^2 which satisfies the boundary condition. This is due to the uniqueness properties of *harmonic functions*: any such v would have to equal $\log(x^2 + y^2)$ for $(x, y) \neq (0, 0)$, which is not defined in $(0, 0)$. This means that even though $\log(x^2 + y^2)$ satisfies the PDE in $\mathbb{R}^2 \setminus \{0\}$ as well as the boundary condition, our approximation must deteriorate as Ω is chosen closer to $(0, 0)$.

In Table 3 we report on our results with various domains at various different distances from the singularity $(0, 0)$ and the results are very good even when the distance is only .01. Figure 19 shows that the errors concentrate on the points that are nearer to the singularity of $\log(x^2 + y^2)$.

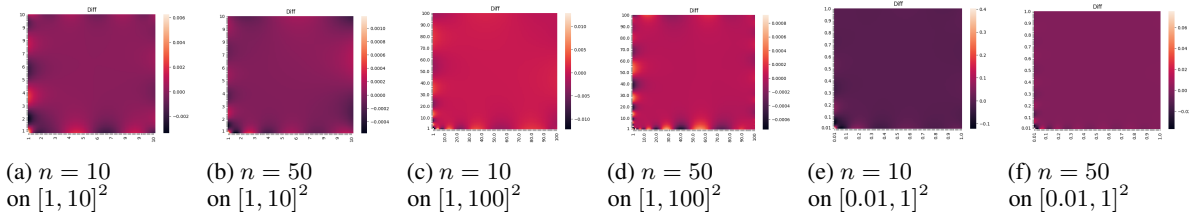


Figure 19: Difference between true and our solution for Laplace’s Equation in Section I. As can be expected, the error concentrates near the singularity at $(0, 0)$ and shows a wave-like behavior, similar to Gibbs phenomenon.

Domain	Absolute L1 Error		Relative L1 Error	
	$n = 10$	$n = 50$	$n = 10$	$n = 50$
$[1, 10]^2$	0.00030	3.6e-6	0.00036	3.59e-5
$[1, 100]^2$	0.00081	7.68e-5	0.00079	6.93e-5
$[0.01, 1]^2$	0.00875	0.00085	0.00642	0.00063

Table 3: We demonstrate how good is our local approximation of a function that is not a global solution due to a singularity at $(0, 0)$. We use 10000 data points and $n = 10$ or $n = 50$ basis elements. We emphasize that the error is really small, despite the distance between the domain and the singularity point being very small.